25. Zhou Z, Peng X, Insolera R, Fink DJ, Mata M. IL-10 promotes neuronal survival following spinal cord injury. *Exp Neurol* 2009; **220**: 183–190.
26. Saraiva M, Christensen JR, Veldhoen M, Murphy TL, Murphy KM, O'Garra A. Interleukin-10 production by Th1 cells requires interleukin-12-induced STAT4 transcription factor and ERK MAP kinase activation by high antigen dose. *Immunity* 2009; **31**: 209–219.
27. Ishii H, Kubo T, Kumanogoh A, Yamashita T. Th1 cells promote neurite outgrowth from cortical neurons *via* a mechanism dependent on semaphorins. *Biochem Biophys Res Commun* 2010; **402**: 168–172.
28. Shaw MH, Freeman GJ, Scott MF, Fox BA, Bzik DJ, Belkaid Y *et al.* Tyk2 negatively regulates adaptive Th1 immunity by mediating IL-10 signaling and promoting IFN-gamma-dependent IL-10 reactivation. *J Immunol* 2006; **176**: 7263–7271.
29. Wong G, Goldshmit Y, Turnley AM. Interferon-gamma but not TNF alpha promotes neuronal differentiation and neurite outgrowth of murine adult neural stem cells. *Exp Neurol* 2004; **187**: 171–177.
30. Baron R, Nemirovsky A, Harpaz I, Cohen H, Owens T, Monsonego A. IFN-gamma enhances neurogenesis in wild-type mice and in a mouse model of Alzheimer's disease. *FASEB J* 2008; **22**: 2843–2852.
31. Butovsky O, Ziv Y, Schwartz A, Landa G, Talpalar AE, Pluchino S *et al.* Microglia activated by IL-4 or IFN-gamma differentially induce neurogenesis and oligodendrogenesis from adult stem/progenitor cells. *Mol Cell Neurosci* 2006; **31**: 149–160.
32. Shechter R, London A, Varol C, Raposo C, Cusimano M, Yovel G *et al.* Infiltrating blood-derived macrophages are vital cells playing an anti-inflammatory role in recovery from spinal cord injury in mice. *PLoS Med* 2009; **6**: e1000113.
33. Kigerl KA, Gensel JC, Ankeny DP, Alexander JK, Donnelly DJ, Popovich PG. Identification of two distinct macrophage subsets with divergent effects causing either neurotoxicity or regeneration in the injured mouse spinal cord. *J Neurosci* 2009; **29**: 13435–13444.
34. Horino J, Fujimoto M, Terabe F, Serada S, Takahashi T, Soma Y *et al.* Suppressor of cytokine signaling-1 ameliorates dextran sulfate sodium-induced colitis in mice. *Int Immunol* 2008; **20**: 753–762.
35. Hirotani T, Lee PY, Kuwata H, Yamamoto M, Matsumoto M, Kawase I *et al.* The nuclear IkappaB protein IkappaBNS selectively inhibits lipopolysaccharide-induced IL-6 production in macrophages of the colonic lamina propria. *J Immunol* 2005; **174**: 3650–3657.
36. Engesser-Cesar C, Anderson AJ, Basso DM, Edgerton VR, Cotman CW. Voluntary wheel running improves recovery from a moderate spinal cord injury. *J Neurotrauma* 2005; **22**: 157–171.
37. Serada S, Fujimoto M, Mihara M, Koike N, Ohsugi Y, Nomura S *et al.* IL-6 blockade inhibits the induction of myelin antigen-specific Th17 cells and Th1 cells in experimental autoimmune encephalomyelitis. *Proc Natl Acad Sci USA* 2008; **105**: 9041–9046.
38. Kitayama M, Ueno M, Itakura T, Yamashita T. Activated microglia inhibit axonal growth through RGMa. *PLoS One* 2011; **6**: e25234.

Cell Adhesion & Migration 7:3, 304–314; May/June 2013; © 2013 Landes Bioscience

Substrate-attached materials are enriched with tetraspanins and are analogous to the structures associated with rear-end retraction in migrating cells

Masashi Yamada,[1] Gabriele Mugnai,[2] Satoshi Serada,[3] Yoshiko Yagi,[1] Tetsuji Naka,[3] and Kiyotoshi Sekiguchi[1,*]

[1]Laboratory of Extracellular Matrix Biochemistry; Institute for Protein Research; Osaka University; Suita, Japan; [2]Department of Experimental Pathology and Oncology; University of Florence; Florence, Italy; [3]Laboratory for Immune Signal; National Institute of Biomedical Innovation; Ibaraki, Japan

Keywords: focal adhesion, integrin, CD9, ganglioside, cell migration, proteomics

Abbreviations: BSA, bovine serum albumin; DMEM, Dulbecco's modified Eagle's medium; ECM, extracellular matrix; FBS, fetal bovine serum; LC-MS/MS, liquid chromatography coupled with tandem mass spectrometry; mAb, monoclonal antibody; pAb, polyclonal antibody; PBS, phosphate-buffered saline; SAM, substrate-attached material; TBS, Tris-buffered saline

Substrate-attached materials (SAMs) are cellular feet that remain on substrates after the treatment of adherent cells with EGTA. SAMs are thought to contain cell adhesion machineries, but their biochemical properties have not been addressed in detail. To gain insight into the molecular mechanisms operating in cell adhesions, we comprehensively identified the protein components of SAMs by liquid chromatography coupled with tandem mass spectrometry, followed by immunoblot analysis. We found that the tetraspanins CD9, CD81, and CD151 were enriched in SAMs along with other transmembrane proteins that are known to associate with tetraspanins. Notably, integrins were detected in SAMs, but the components of focal adhesions were scarcely detected. These observations are reminiscent of the "footprints" that remain on substrates when the retraction fibers at the rear of migrating cells are released, because such footprints have been reported to contain tetraspanins and integrins but not focal adhesion proteins. In support of this hypothesis, the formation of SAMs was attenuated by inhibitors of ROCK, myosin II and dynamin, all of which are known to participate in rear-end retraction in migrating cells. Furthermore, SAMs left on collagen-coated substrates were found by electron microscopy to be fewer and thinner than those on laminin-coated substrates, reflecting the thin and fragile retraction fibers of cells migrating on collagen. Collectively, these results indicate that SAMs closely resemble the footprints and retraction fibers of migrating cells in their protein components, and that they are yielded by similar mechanisms.

Introduction

Cell adhesions on extracellular matrices (ECMs) are involved in the regulation of a variety of biological processes, including cell growth, differentiation, survival, and migration. The interaction of cells with ECMs is mediated mainly by integrins, heterodimers composed of non-covalently associated α- and β-subunits.[1] The binding of integrins to ECMs stimulates their clustering and the formation of multiprotein complexes called focal adhesions. Focal adhesions perform both mechanical and signaling functions that control cytoskeletal rearrangements and various cellular responses.[2,3] The mechanical functions are mediated by focal adhesion components such as talin, kindlin, α-actinin, and vinculin, which connect the actin cytoskeleton to the ECM. The signaling functions are mediated by components such as FAK, Src, paxillin, and ILK, which transmit intracellular signals via the regulation of protein and lipid kinases and GTPases.[1,2] Defects in the regulation of integrin-mediated cell adhesions result in various diseases such as cancer, immune disorders, thrombosis, and skeletal muscle dystrophy.[4-6]

Cell migration is a coordinated process that involves the formation and disassembly of cell adhesion sites together with dynamic changes in the actin cytoskeleton.[7,8] To migrate efficiently, cells must possess an asymmetric morphology with defined leading and trailing edges. Nascent focal adhesions are newly formed at the leading edge, following which they either mature into stabilized adhesions or turnover. In contrast, focal adhesions at the trailing edge are disassembled during rear-end retraction, which allows the cell body to translocate. The regulation of adhesion disassembly at the trailing edge is less well understood than the maturation and turnover of adhesions at the leading edge.

*Correspondence to: Kiyotoshi Sekiguchi; Email: sekiguch@protein.osaka-u.ac.jp
Submitted: 01/18/13; Revised: 05/14/13; Accepted: 05/15/13
http://dx.doi.org/10.4161/cam.25041

In the 1970s, substrate-attached materials (SAMs) were found to remain tightly bound to substrates when adherent cells were detached with the Ca^{2+}-specific chelator, EGTA.[9] Morphological investigations revealed that SAMs are composed of cell-surface regions rich in adhesion sites.[10,11] Biochemical analyses showed that SAMs contain relatively large amounts of cell surface components that participate in cell adhesion such as cellular fibronectin,[12] proteoglycans,[13,14] and gangliosides.[15,16] Detailed analysis of the molecular composition of SAMs may therefore provide insight into the molecular mechanisms underlying the cellular events regulated by cell adhesion, but the molecular properties of SAMs have remained largely uninvestigated over the past two decades.

In the present study, we sought to define the molecular composition of SAMs by proteomic analysis using liquid chromatography coupled with tandem mass spectrometry (LC-MS/MS) to investigate the mechanisms underlying the regulation of cellular responses by cell–ECM adhesions. We found that SAMs contain large amounts of tetraspanins and their associated proteins, but not focal adhesion proteins, and thus resemble the footprints and retraction fibers of migrating cells that are also enriched with tetraspanins.[17,18] In addition, the formation of SAMs was dependent on actomyosin activity and dynamin-mediated endocytosis, as is the case with rear-end retraction in migrating cells.[19,20] Our findings revealed that SAMs are closely correlated with rear-end retraction in migrating cells.

Results

Proteomic analysis of SAMs. To comprehensively identify the protein components of SAMs, A549 cells that had been cultured on laminin-511 in serum-free conditions were treated with EGTA to prepare SAMs. Scanning electron microscopy showed that EGTA treatment evoked the retraction and rounding of cells, leaving long, thin and branched protrusions (SAMs) firmly bound to the substrates (**Fig. 1A**). These results are consistent with a previous report,[16] in which SAMs were prepared from rat hepatoma CMH5123 cells and examined by scanning electron microscopy. To perform proteomic analysis, SAMs were harvested from the dishes with SDS after the detachment of cells by treatment with EGTA. Determination of the protein content in SAMs and detached cells indicated that only 0.88 ± 0.03% (n = 3) of the total cellular protein was recovered in SAMs. Separation of the SAM proteins by SDS-PAGE showed that their banding pattern was obviously different from that of proteins in detached cells (**Fig. 1B**).

The SAM proteins separated by SDS-PAGE were subjected to in-gel digestion with trypsin, and the resulting peptides were extracted from the gels and analyzed by LC-MS/MS. LC-MS/MS analyses of three independent SAM preparations resulted in the detection of 1971, 3018, and 2691 proteins per analysis (**Tables S1–3**), 1739 proteins of which were reproducibly detected (**Table S4**). In the present study, we focused on plasma transmembrane proteins, because they should include cell adhesive molecules and regulators, which are important in initiating cellular responses at the interface of cell–ECM interactions. We found

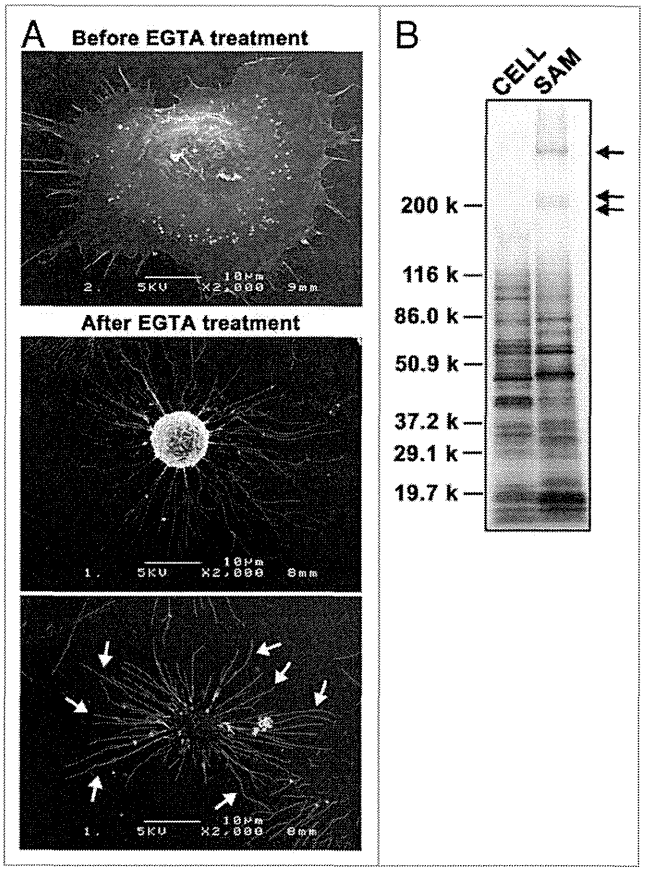

Figure 1. Substrate-attached materials on laminin-511. (**A**) A549 cells were cultured on laminin-511-coated dishes for 2h30min. Cells were then treated with EGTA for 15 min and fixed. Scanning electron micrographs were obtained as described in Materials and Methods. Arrows indicate SAMs. (**B**) SAMs were prepared after detaching the cells by treatment with EGTA as described in Materials and Methods, following which they were separated by SDS-PAGE under reducing conditions and silver-stained. Lysates were also prepared from detached cells (CELL) and analyzed by SDS-PAGE. The positions of molecular weight markers are shown on the left. Arrows indicate laminin-511, which was used to coat dishes.

that the plasma transmembrane proteins thus detected in SAMs include integrins, CD44 and Lu/BCAM, which also have been detected in tetraspanin-enriched microdomains (also referred to as the tetraspanin web) (**Table 1**; **Table S4**).[21-23] Notably, protein components of focal adhesions were not detected in SAMs, except for α-parvin (**Table S4**).

Enrichment of tetraspanins in SAMs. To further examine the occurrence of proteins that have been shown to associate with focal adhesions and tetraspanin-enriched microdomains in SAMs, we performed immunoblot analysis (**Fig. 2A**). Talin, α-actinin, vinculin, paxillin, and α-parvin, which are components of focal adhesions, were scarcely detected in SAMs, as was the case with actin. In contrast, the two tetraspanins CD9 and CD81 were significantly enriched in SAMs when compared with lysates prepared from detached cells, although another tetraspanin, CD151, was not concentrated in SAMs but was

Table 1. Plasma transmembrane proteins detected by LC-MS/MS analysis of SAMs

Category	Protein	Gene	Association with TSPANs[†]
Tetraspanins	CD9 antigen	(CD9)	
	CD81 antigen	(CD81)	
	Tetraspanin-4	(TSPAN4)	
	Tetraspanin-14	(TSPAN14)	
Integrins	Integrin α3	(ITGA3)	+
	Integrin α6	(ITGA6)	+
	Integrin αv	(ITGAV)	+
	Integrin β1	(ITGB1)	+
	Integrin β5	(ITGB5)	+
Ig superfamily	Ig superfamily member 8/EWI2	(IGFSF8)	+
	Lutheran blood group glycoprotein	(BCAM)	+
	CD166 antigen	(ALCAM)	+
	Basigin/CD147[‡]	(BSG)	NR
	Poliovirus receptor/NECL-5	(PVR)	NR
Cell adhesion molecules	CD44 antigen	(CD44)	+
	Cadherin-1	(CDH1)	+
	Claudin-1	(CLDN1)	+
Receptors	Transferrin receptor protein 1	(TFRC)	NR
	Renin receptor	(ATP6AP2)	NR
	Ephrin type-A receptor 2	(EPHA2)	NR
	Neuropilin-1	(NRP1)	NR
	Receptor-type Tyr-protein phosphatase F	(PTPRF)	NR
	Scavenger receptor class B member 1	(SCARB1)	NR
	Plasminogen receptor (KT)	(C9orf46)	NR
	Retinoic acid-induced protein 3	(GPRC5A)	NR
	Endothelial protein C receptor	(PROCR)	NR
Proteases	Disintegrin and metalloproteinase domain-containing protein 10	(ADAM10)	+
	Matrix metalloproteinase-14/MT1-MMP	(MMP14)	+
	Nicastrin	(NICA)	+
Transporters	4F2 cell-surface antigen heavy chain[¶]	(SLC3A2)	+
	Large neutral amino acids transporter small subunit 1	(SLC7A5)	NR
	Na^+-coupled neutral amino acid transporter 2	(SLC38A2)	NR
	Na^+/K^+-transporting ATPase subunit β -1	(ATP1B1)	NR
Others	Myoferlin	(MYOF)	NR
	Protein LYRIC	(MTDH)	NR
	Extended synaptotagmin-2	(ESYT2)	NR
	Proteolipid protein 2	(PLP2)	NR
	Amphiregulin	(AREG)	NR
	Amyloid β A4 protein	(APP)	NR
	Kunitz-type protease inhibitor 2	(SPINT2)	NR

The listed plasma transmembrane proteins were reproducibly detected in three independent LC-MS/MS analyses of SAMs prepared from A549 cells cultured on laminin-511. [†]+ indicates the proteins that have been shown to interact with tetraspanins.[49-60] NR, not reported. [‡]Protein reported to interact with integrin α3β1 and α6β1.[61] [¶]Protein reported to interact with integrin β1.[62,63] See also **Table S4**.

detected at a relatively high level. The lower abundance of CD151 may explain why CD151 was detected in only one of three proteomic analyses (**Table S2**). Alternatively, the failure of LC-MS/MS analysis may be due to the difficulty in the detection of tetraspanins by LC-MS/MS, possibly because a major part of their sequence is transmembranous.[24] Integrin β1, integrin α3, CD44, and ADAM10, which are known to be associated with tetraspanins, were also detected in SAMs at relatively high levels

compared with focal adhesion proteins. Similar results, including the detection of large quantities of tetraspanins, were also obtained with HT-1080 cells (**Fig. S1**). Consistent with these results, SAMs remaining on laminin-coated surfaces after EGTA treatment were positively immunostained with anti-CD9, anti-CD81, and anti-CD151 antibodies (**Fig. 2B**). The signals for CD81 were less pronounced than those for CD9 and CD151, possibly due to the reduced reactivity of the anti-CD81 antibody toward formaldehyde-fixed SAMs. These results indicate that SAMs contain tetraspanins and their associated proteins, but not focal adhesion proteins.

It has been reported that migrating cells exhibit retraction fibers on their tails and leave behind "footprints" or "migration tracks" that contain integrins and tetraspanins, but not focal adhesion components.[17,25-27] Immunofluorescence staining of A549 cells migrating on laminin-511 showed that CD9, CD81, and CD151 were detected discontinuously but throughout retraction fibers (**Fig. 3**), overlapping with F-actin. It should be noted that F-actin signals retracted more readily than tetraspanin signals, leaving behind the tetraspanin$^+$/F-actin$^-$ regions. These findings raise the possibility that SAMs are closely related to footprints and retraction fibers based on not only their morphology but also their protein composition.

Involvement of actomyosin activity and dynamin-dependent endocytosis in the formation of SAMs. To assess whether the process of SAM formation resembles that of rear-end retraction in migrating cells, we examined the effects of inhibiting actomyosin contractility, which is critically involved in rear-end retraction in migrating cells.[19] When cells cultured on laminin-511 were treated with EGTA in the presence of Y-27632 and blebbistatin, inhibitors of ROCK and myosin II, respectively, cell retraction and detachment were significantly attenuated, leaving the cells spread on the substrates (**Fig. 4**). However, even in the presence of the inhibitors, EGTA-treated cells extended many thin protrusions at their peripheries, indicating that these inhibitors delay, rather than completely block, the formation of SAMs. In A549 cells migrating on laminin-511, these inhibitors also disturbed the detachment of retraction tails, thereby stimulating the elongation of the retraction tails (**Vids. S1–S3**). We also investigated whether clathrin-dependent endocytosis, which is also involved in rear-end retraction in migrating cells,[28,29] participates in cell retraction following EGTA treatment. As shown in **Figure 5**, the cell retraction and detachment were blocked by the addition of dynasore, a dynamin inhibitor, which inhibits clathrin-dependent endocytosis.[30] As with Y-27632 and blebbistatin, dynasore did not completely prevent, but rather retarded, the formation of SAMs. The migration of A549 cells on laminin-511 was also suppressed by dynasore with an apparent loss of front-rear polarity and retraction tails (**Vid. S4**). These results support the possibility that SAMs are analogous to retraction fibers and footprints, and that they are formed and left on the substrates through similar molecular processes.

Morphological similarities between SAMs and retraction fibers on different ECM proteins. To further address the similarity between SAMs and retraction fibers and footprints, we compared cell migration on laminin-511 and type I collagen by time-lapse phase-contrast microscopy. Cells on laminin-511 showed thick and stable retraction fibers on their tails, although the retraction fibers of cells on type I collagen were thin and fragile (**Fig. 6; Vids. S5 and S6**). The diameters of the retraction fibers were 0.357 μm ± 0.058 (n = 133) on laminin-511 and 0.232 μm ± 0.035 on type I collagen (n = 105). Consistent with these results, scanning electron microscopy of EGTA-treated

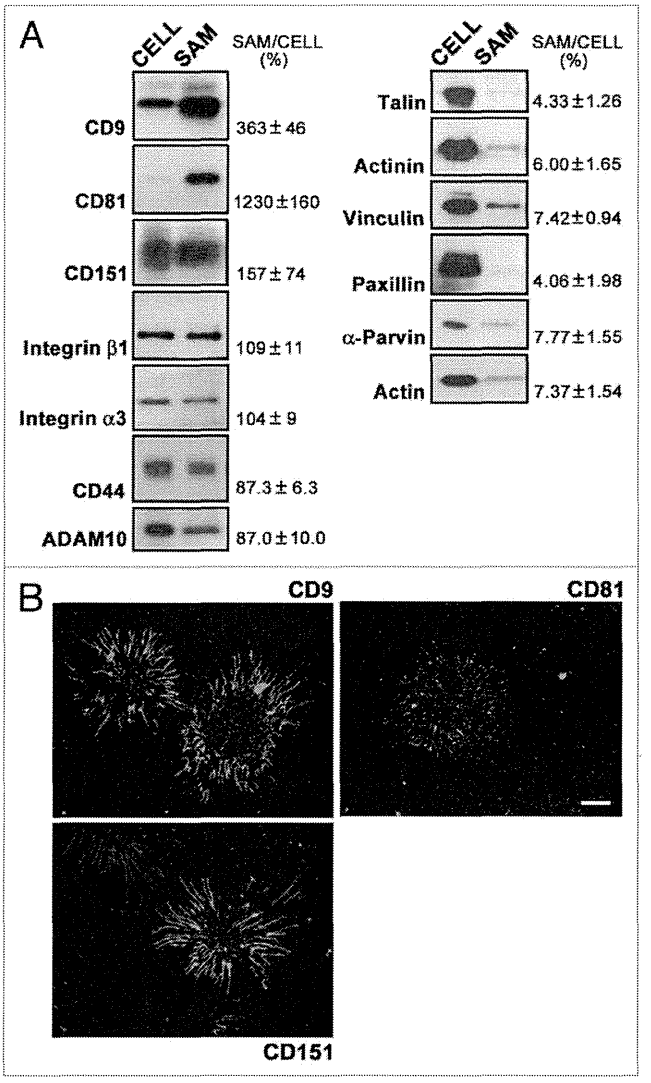

Figure 2. Detection of tetraspanins and their associated proteins in SAMs. (**A**) SAMs were prepared following the treatment of A549 cells cultured on laminin-511 with EGTA as described in Materials and Methods. Lysates (CELL) were also prepared from the cells detached by the EGTA treatment. SAMs and lysates were separated by SDS-PAGE, and subsequently immunoblotted with the antibodies indicated on the right of the blots. Data are representative of three separate experiments. The relative intensities of bands detected in SAMs to those in cell lysates are shown on the right. Values represent means ± SD from three independent experiments. (**B**) A549 cells cultured on laminin-511 were treated with EGTA. SAMs remaining on the substrates were immunostained with anti-CD9, anti-CD81, and anti-CD151 antibodies as described in Materials and Methods. Bar represents 10 μm.

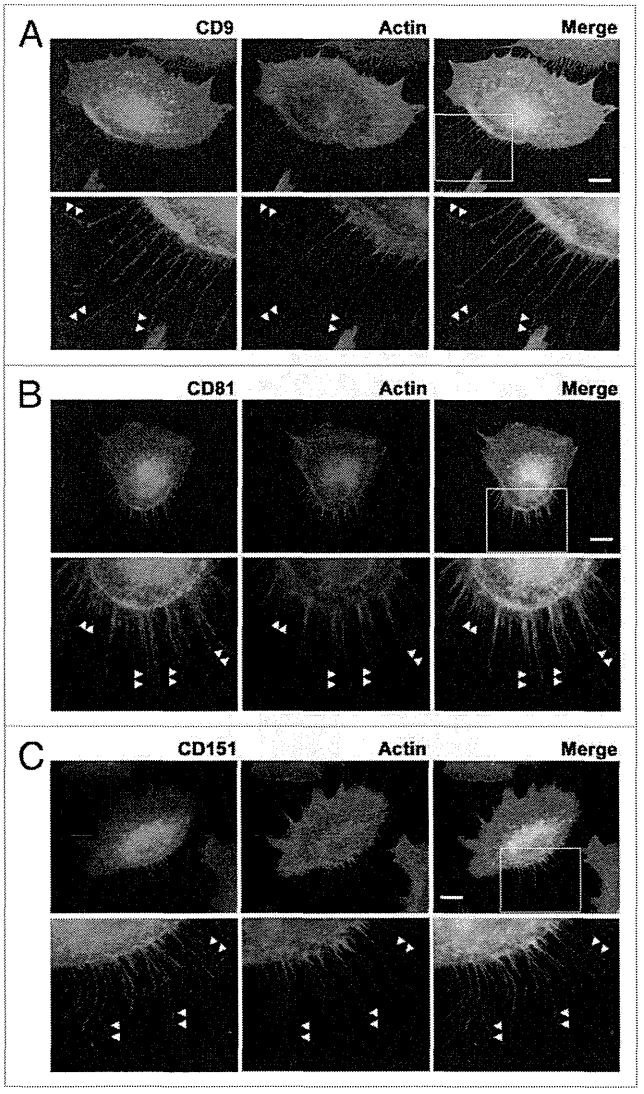

Figure 3. Localization of CD151 in retraction fibers in migrating cells. A549 cells migrating on laminin-511 were stained with anti-CD9 (**A**), anti-CD81 (**B**), and anti-CD151 (**C**) antibodies (green) and rhodamine-phalloidin (red) as described in Materials and Methods. The lower panels show high magnification views of the boxed areas. Arrowheads indicate tetraspanin-positive but F-actin-negative regions in retraction fibers. Bars represent 10 μm.

cells on laminin-511 and type I collagen demonstrated that the SAMs on laminin-511 were greater in number and thicker than those on type I collagen (**Fig. 7A and B**). Immunoblot analysis showed that greater amounts of integrins β1 and α3, CD9, CD81, CD151, ADAM10, and CD44 were detected in SAMs on laminin-511 than in SAMs on type I collagen (**Fig. 7C**). These results are in agreement with the morphological distinctions between the SAMs on laminin-511 and type I collagen. In contrast, the cytoskeletal protein, keratin 18, the RNA-binding protein, G3BP, the nuclear protein, histone H3, and the mitochondrial protein, prohibitin, were detected at almost the same levels in SAMs remaining on laminin-511 and type I collagen. It seems likely, therefore, that integrins β1 and α3, CD9, CD81, CD151, ADAM10, and CD44 are intrinsic components of SAMs, while keratin 18, G3BP, histone H3, and prohibitin, which were detected in large amounts by mass spectrometric analysis, are entrapped in SAMs independently of the mechanism operating in cell retraction.

Discussion

SAMs were discovered in the 1970s as cellular feet that remained on substrates after detachment of cells with EGTA, although there have been few reports on SAMs in the past two decades. In the present study, we focused on SAMs as cell–ECM adhesion machineries, and performed the comprehensive determination of their protein components to uncover the molecular mechanisms underlying cellular events regulated by cell–ECM adhesions. Our data indicate that SAMs are closely related to the retraction fibers and footprints that appear during rear-end retraction in migrating cells, thus revealing new aspects of SAMs as cell adhesion structures.

At the rear of migrating cells, retraction fibers are observed during rear-end detachment. At the tips of these fibers, "membrane ripping" occurs, thereby leaving footprints on substrates.[25,31] We found that CD9, CD81, and CD151 were enriched in SAMs. Integrins were also recovered in SAMs, but focal adhesion components, including talin, α-actinin, vinculin, paxillin, and α-parvin, were scant. These properties of SAMs are reminiscent of those of footprints and retraction fibers. It has been reported that footprints contain high amounts of integrins in various types of cells, including keratinocytes and fibroblasts.[25-27] Focal adhesion constituents such as talin and vinculin are scarcely present in footprints. Peñas et al.[17] reported that tetraspanins such as CD9 and CD81 exist at high levels in the footprints of keratinocytes. In human prostate cancer Du145 cells, CD81 was shown to be present in footprints and retraction fibers in which F-actin was scarcely detected.[18] Consistent with these reports, we observed that in A549 cells migrating on laminin-511, CD9, CD81, and CD151 were detected throughout retraction fibers, and even in the regions near their tips where F-actin was scant. It is conceivable, therefore, that SAMs are structurally analogous to the footprints and retraction fibers of migrating cells.

Inhibition of ROCK and myosin II by Y-27632 and blebbistatin attenuated the formation of SAMs by EGTA treatment. It is known that Rho/ROCK signaling mediates the retraction of the trailing edges of cells and is implicated in adhesion disassembly during cell detachment.[19] Inhibition of Rho kinase induces an elongated morphology with impaired rear-end detachment.[32] In addition, fibroblasts deficient in myosin IIA show impaired adhesion disassembly and rear-end detachment.[33] We also observed similar phenomena in A549 cells migrating on laminin-511 in the presence of Y-27632 and blebbistatin by time-lapse microscopy. Therefore, rear-end retraction in migrating cells and SAM formation by EGTA treatment may be driven by similar machineries that involve actomyosin activity.

We also found that the formation of SAMs was suppressed by dynasore, an inhibitor of dynamin, which also participates

in rear-end retraction by mediating clathrin-dependent endocytosis.[8,20,28] By time-lapse microscopy, we observed that dynasore effectively inhibited the migration of A549 cells on laminin-511. It has been reported that the endocytosis and recycling of integrin αvβ3 contributes to adhesion release in neutrophils migrating on vitronectin.[34] In the migration of mouse fibroblast NIH3T3 and human fibrosarcoma HT1080 cells, clathrin-mediated endocytosis is involved in focal adhesion disassembly.[20,28,29] Taken together, the formation of SAMs and rear-end retraction in migrating cells seem to share similar mechanisms involving actomyosin activity and clathrin-dependent endocytosis.

Scanning electron microscopic observations showed that SAMs on type I collagen-coated substrates were fewer and thinner than those on laminin-511-coated substrates. Consistent with these results, tetraspanins and their associated proteins were detected at significantly reduced levels in SAMs on type I collagen compared with SAMs on laminin-511. In contrast, the cytoskeletal protein, keratin 18, the nuclear protein, histone H3, and the mitochondrial protein, prohibitin, were detected in large amounts in SAMs irrespective of the type of substrate. These observations make it likely that the nuclear, mitochondrial, and cytoskeletal proteins frequently detected in our LC-MS/MS analyses are not intrinsic components of SAMs, but this possibility needs to be confirmed extensively by immunoblot analysis of individual proteins in SAMs prepared on laminin-511 and type I collagen.

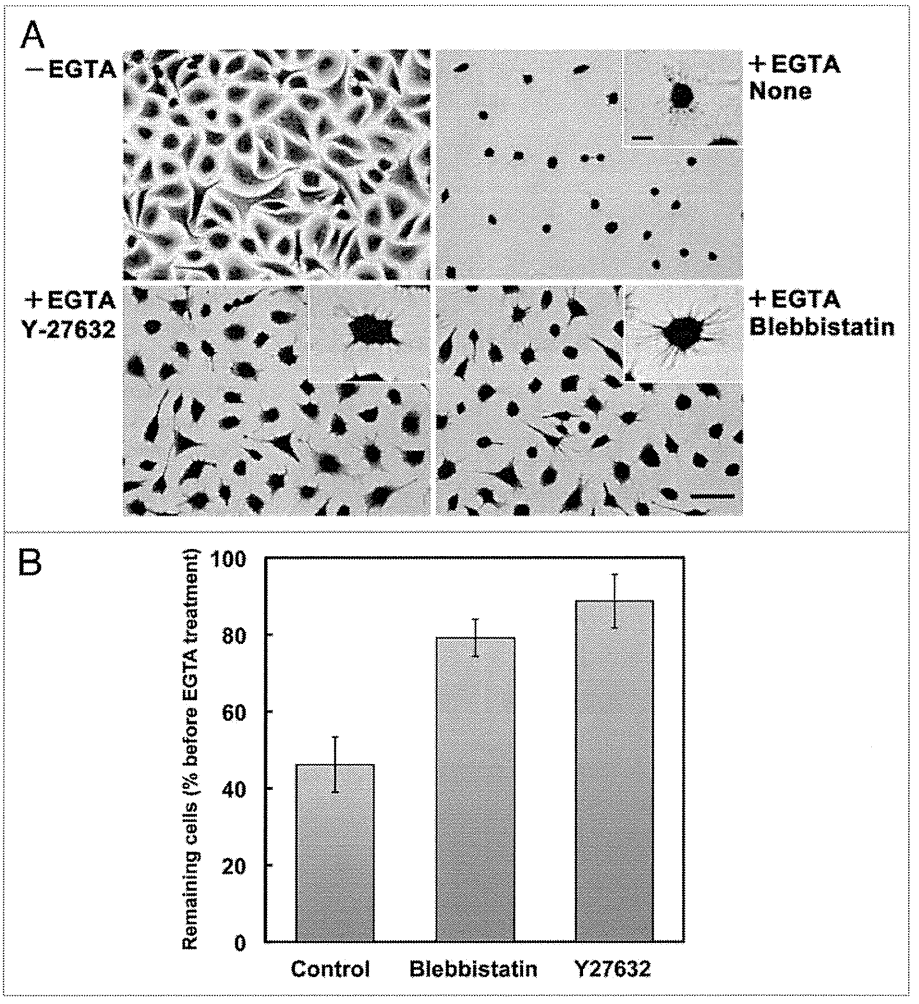

Figure 4. Involvement of actomyosin contractility in the formation of SAMs. (**A**) A549 cells were allowed to adhere to laminin-511 for 2h30min (−EGTA). Then, cells were treated with EGTA (+EGTA) for 15 min in the absence (*None*) or presence of 10 μM Y-27632 or 20 μM (±)-blebbistatin, following which they were stained with toluidine blue. Bar represents 50 μm. High-magnification images are shown in the insets (bar indicates 10 μm). (**B**) Cells remaining on the substrates were quantified as described in Materials and Methods. Values represent the mean ± SD ($n = 3$).

Tetraspanins, which possess four transmembrane domains, are present in different combinations in almost all types of cells and tissues, and have been implicated in diverse cellular functions involving cell–cell and cell–substratum interactions.[21-23] Tetraspanins associate with each other and with other transmembrane proteins, e.g., integrins and immunoglobulin superfamily proteins, thereby forming multimolecular membrane microdomains, often referred to as a tetraspanin-enriched microdomain or the tetraspanin web. Many reports have suggested that tetraspanins are involved in the regulation of cell migration,[21,35] although the mechanisms involved remain largely unknown. Several lines of evidence indicate that the deregulation of tetraspanin expression is associated with cancer metastasis.[36-38] Zijlstra et al.[39] have reported that an anti-CD151 mAb, which blocks metastasis, prevents rear-end detachment during the migration of human epidermoid carcinoma cells, suggesting the involvement of tetraspanins in rear-end retraction in migrating cells. Tetraspanins, which are major components of SAMs, may also participate in SAM formation upon EGTA treatment. Further studies on the roles of tetraspanins in SAM formation will provide a better understanding of the mechanisms underlying rear-end retraction in migrating cells.

It has been reported that GD2/GD3 gangliosides are required for the detection of CD151 in cellular microprocesses left on substrates after the detachment of COS-7 cells by treatment with EDTA.[40] Gangliosides have been shown to associate with several tetraspanins, i.e., CD9 and CD82, and thereby regulate

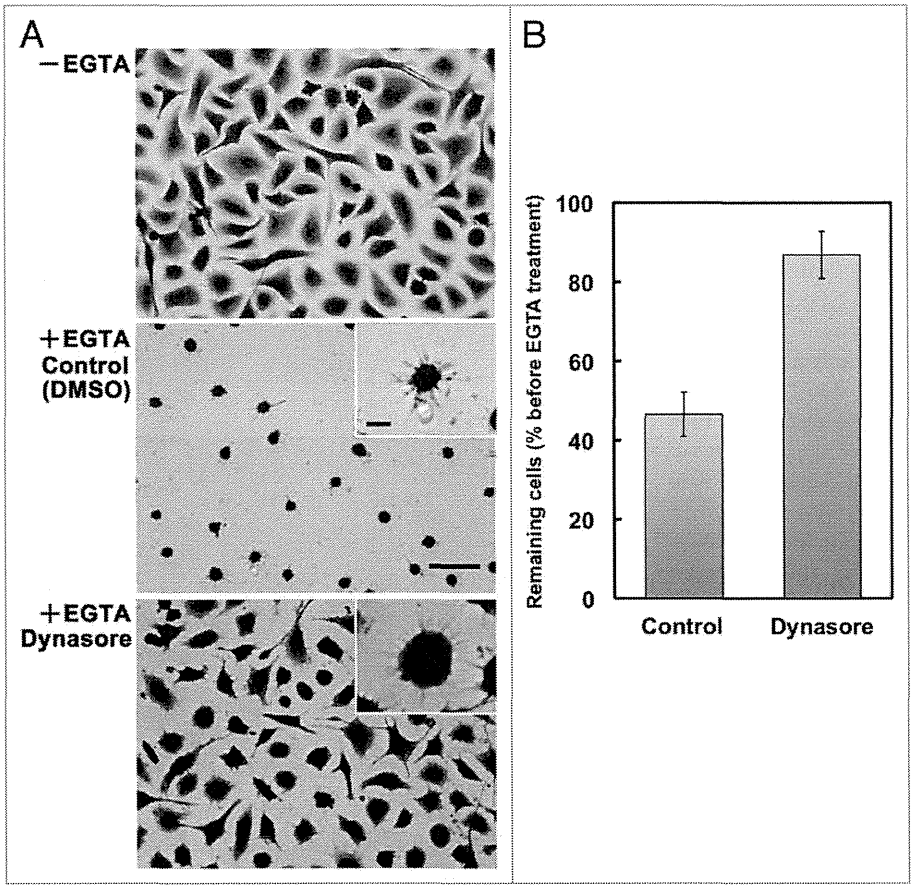

Figure 5. Involvement of dynamin activity in the formation of SAMs. (**A**) A549 cells were allowed to adhere to laminin-511 for 2h30min (−EGTA). Then, cells were treated with EGTA (+EGTA) for 15 min in the presence of 0.1% DMSO (Control) or 100 μM dynasore, following which they were stained with toluidine blue. Bar represents 50 μm. High-magnification images are shown in the insets (bar indicates 10 μm). (**B**) Cells remaining on the substrates were quantified as described in Materials and Methods. Values represent the mean ± SD ($n = 3$).

protein–protein interactions in tetraspanin-enriched microdomains.[41-44] In addition, SAMs contain various kinds of gangliosides, including GD2 and GD3.[15,16] Thus, localization of tetraspanins may, at least in part, be because of their association with gangliosides. Given that gangliosides are known to participate in the regulation of cell migration through integrins,[45] tetraspanins and gangliosides may cooperatively participate in rear-end retraction in migrating cells.

In summary, our results raise the possibility that the molecular mechanism of SAM formation mimics that of rear-end retraction in migrating cells. Given that the regulation of cell adhesion at the trailing edges is less well defined than that at the leading edges, the analysis of SAMs will provide novel insights into the mechanisms of cell migration. In addition, it has been proposed that the trailing edge of a cell drives cell migration by forming a defined rear prior to the formation of polarized cell protrusions.[46] Further analysis of SAMs could enable the molecular mechanisms underlying the formation of front-rear polarization, as well as rear-end retraction, in migrating cells to be elucidated.

Materials and Methods

Cell culture, ECM proteins, antibodies, and reagents. A549 human lung adenocarcinoma and HT-1080 human fibrosarcoma cells were maintained in 10-cm dishes in Dulbecco's modified Eagle's medium (DMEM, Sigma) supplemented with heat-inactivated 10% (v/v) fetal bovine serum (FBS; JRH Biosciences). The cells were cultured at 37 °C in a humidified atmosphere containing 5% CO_2.

Laminin-511 was purified from the conditioned medium of human choriocarcinoma JAR cells as described previously.[47] Type I collagen was purchased from Nitta Gelatin (Cellmatrix Type I-C).

A mouse monoclonal antibody (mAb) against human CD151 (8C3) was produced as described previously.[48] Anti-CD9 mouse mAb (MM2/57) was purchased from Chemicon; anti-integrin α3 goat polyclonal antibody (pAb), anti-CD81 mouse mAb (5A6), and anti-CD44 rat mAb (IM7) were purchased from Santa Cruz; anti-paxillin mouse mAb, anti-α-actinin mouse mAb, and anti-integrin β1 mouse mAb were from BD Transduction Lab; α-parvin rabbit pAb was from Cell Signaling; anti-actin rabbit pAb, anti-talin mouse mAb (8D4), and anti-vinculin mouse mAb (hVIN-1) were from Sigma; anti-ADAM10 rabbit pAb was from Millipore; peroxidase-conjugated AffiniPure anti-mouse IgG, anti-rabbit IgG, anti-rat IgG, and anti-goat IgG antibodies were from Jackson Immuno Res; Alexa 488-conjugated anti-mouse IgG antibody and rhodamine-labeled phalloidin were from Molecular Probes. Y-27632, (±)-blebbistatin, and dynasore were purchased from Calbiochem.

Preparation of SAMs. Cells were detached from dishes with PBS containing 0.025% trypsin and 1 mM EDTA. For LC-MS/MS, detached cells were washed 3 times with serum-free DMEM containing 10 mM HEPES-NaOH, pH 7.5, resuspended in the same medium, and then plated on dishes that had been coated with 5 nM laminin-511 and blocked with Protein-free Blocking Reagent (Pierce). For immunoblot analysis, cells were prepared and seeded in the same way as for LC-MS/MS, except that medium containing 10 mM HEPES-NaOH, pH 7.5, and 0.5% (w/v) bovine serum albumin (BSA) was used for cell suspension and blocking of the coated dishes. After culture for 2h30min, cells were washed twice with PBS and then once with 1 mM

EGTA, 1 mg/ml glucose in PBS, and treated with 1 mM EGTA, 1 mg/ml glucose in PBS at 37 °C for 20 min. Cells were completely detached by washing 5 times with PBS containing 1 mM EGTA and then 3 times with PBS. Dishes were washed twice with ice-cold PBS containing 0.2% Brij 97 at 4 °C, and further washed 3 times with ice-cold PBS at 4 °C. SAM proteins on dishes were extracted with 0.25% SDS at 37 °C, and then concentrated with centrifugal filter devices (Amicon Ultra-4, Millipore) for analysis by LC-MS/MS and immunoblotting. Cells detached by the EGTA treatment were lysed with 0.25% SDS and used in immunoblot analysis for comparison with SAMs.

Liquid chromatography coupled with tandem mass spectrometry. Protein samples were separated by SDS-PAGE (SDS-PAGE) and then fixed in the gels with 30% methanol, 10% acetic acid. After washing with deionized water, the gels were cut into >20 rectangular pieces and then washed sequentially with 25 mM ammonium bicarbonate containing 50% acetonitrile, 100% acetonitrile, 100 mM ammonium bicarbonate, and 100% acetonitrile. The gel pieces were dried and then incubated with 100 mM ammonium bicarbonate and 10 mM DTT at 56 °C for 45 min. After cooling to room temperature, the DTT solution was replaced with 100 mM ammonium bicarbonate, 55 mM iodoacetamide and the gel pieces were incubated at room temperature for 30 min in the dark. The gel pieces were washed sequentially with deionized water, 25 mM ammonium bicarbonate containing 50% acetonitrile, 100% acetonitrile, 100 mM ammonium bicarbonate, and 100% acetonitrile. After being dried, the gel pieces were subjected to trypsin digestion at 35 °C overnight with XL-TrypKit (Apro Sci.). Following enzymatic digestion, the resulting peptides were extracted sequentially with 5% trifluoroacetic acid containing 50% acetonitrile, and 100% acetonitrile. The peptides were dried and cleaned up with PepClean C-18 Spin Columns (Pierce). The peptides eluted from the columns with 70% acetonitrile were dried and dissolved in 0.1% trifluoroacetic acid.

LC-MS/MS analyses were performed on a LTQ-Orbitrap XL mass spectrometer (Thermo Fisher Scientific) equipped with a nano-ESI source (AMR) and coupled to a Paradigm MG2 pump (Michrom Bioresources) and an autosampler (HTC PAL, CTC Analytics). A spray voltage of 2200 V was applied. Peptide mixtures were separated on a MagicC18AQ column (100 μm × 150 mm, 3.0 μm particle size, 300 Å, Michrom Bioresources) with a flow rate of 500 nl/min. A linear gradient of 5–30% buffer B in buffer A for 80 min, 30–95% buffer B in buffer A for 10 min, 95% buffer B and 5% buffer A for 4 min, and finally decreasing to 5% buffer B in buffer A, was employed (buffer A = 0.1% formic acid in 2% acetonitrile, buffer B = 0.1% formic acid in 90% acetonitrile). Intact peptides were detected in the Orbitrap at 60 000 resolution. For LC-MS/MS analysis, 10 precursor ions were selected for subsequent MS/MS scans in a data-dependent acquisition mode following each full scan (m/z, 450–1800). A lock mass function was used for the LTQ-Orbitrap to obtain constant mass accuracy during gradient analysis.

Peptides and proteins were identified by means of an automated database search using Proteome Discoverer v.1.3 (Thermo Fisher Scientific) with the MASCOT algorithm against the SwissProt protein database (version 2012_06, 536489 sequences). Taxonomy was set to *Homo sapiens* (20 312 entries). Search parameters for peptide and MS/MS mass tolerance were 10 ppm and 0.8 Da, respectively, with allowance for two missed cleavages in the trypsin digest. Carbamidomethylation of cysteine was set as a fixed modification and oxidation of methionines was allowed as a variable modification. MASCOT results were filtered with the integrated Percolator based filter using a false discovery rate of <1% (based on PSMs).

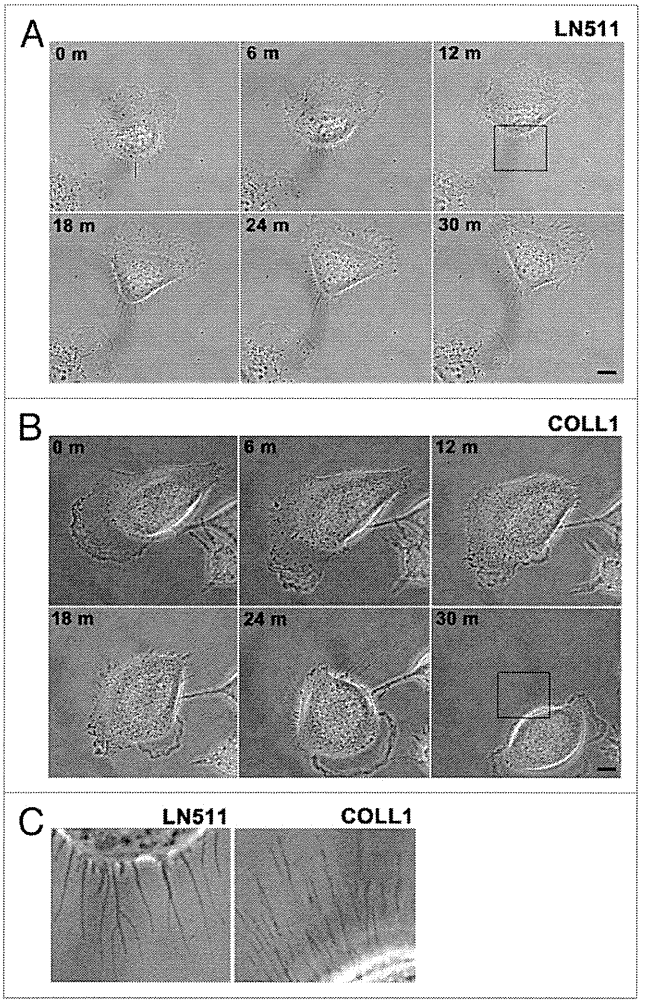

Figure 6. Morphological differences in retraction fibers in cells migrating on laminin-511 or type I collagen. (**A and B**) Migration of A549 cells on laminin-511 (LN511, [**A**]) or type I collagen (COLL1, [**B**]) was recorded by time-lapse microscopy as described in Materials and Methods. Bars represent 10 μm. See also **Vids. S1 and S2**. (**C**) The left and right panels show high magnification views of the areas boxed in (**A and B**), respectively. The data are representative of 43 and 21 cells migrating on laminin-511 or type I collagen, respectively.

Immunoblotting. The protein concentrations of samples were determined using BCA Protein Assay Reagent (Pierce). Samples containing equal amounts of protein were separated by SDS-PAGE and transferred onto polyvinylidene fluoride membranes (Millipore) in 0.1 M Tris base, 0.192 M glycine, and 20% (v/v)

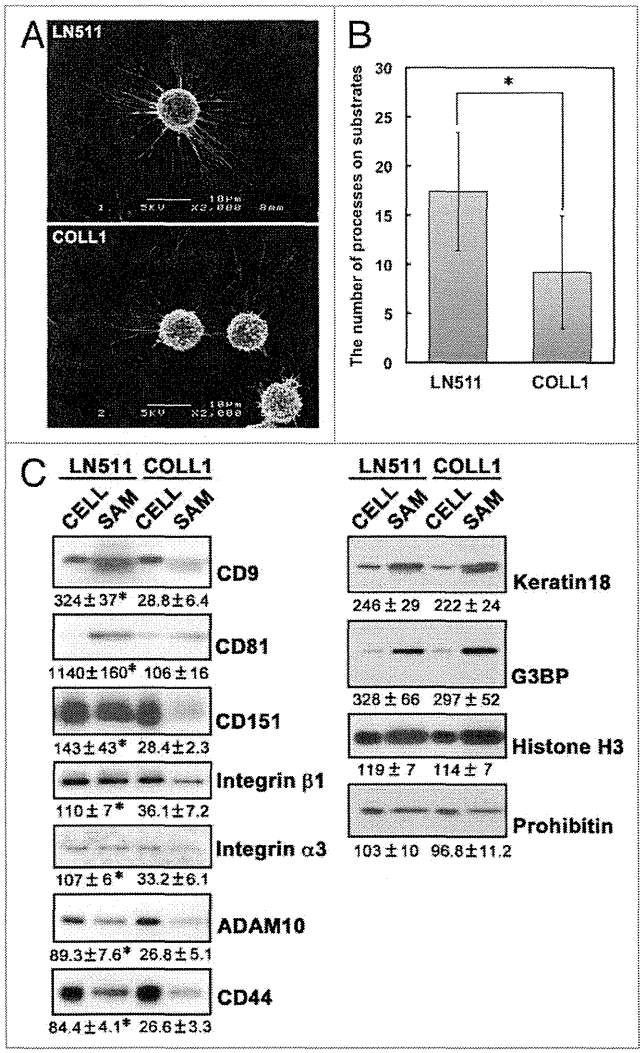

Figure 7. Differences in SAMs remaining on laminin-511 and type I collagen. (**A**) A549 cells were cultured on laminin-511 (LN511)- or type I collagen (COLL1)-coated dishes for 2h30min. The cells were then treated with EGTA for 15 min and fixed. Scanning electron micrographs were obtained as described in Materials and Methods. (**B**) The number of cell processes per cell was counted in the electron micrographs. Values represent the mean ± SD ($n = 27$ for laminin-511 and $n = 28$ for type I collagen; $^*P < 0.00001$, the Student t-test). (**C**) SAMs were prepared following EGTA treatment of A549 cells cultured on laminin-511 (LN511) or type I collagen (COLL1) as described in Materials and Methods. Lysates (CELL) were also prepared from the cells detached by the EGTA treatment. These proteins were then immunoblotted with the antibodies indicated on the right of the blots. Data are representative of three separate experiments. The relative intensities of bands detected in SAMs to those in cell lysates are shown on the right. Values represent means ± SD from three independent experiments. Statistical analysis was performed using the Student t-test, $^*P < 0.05$.

methanol using a semi-dry electrophoretic transfer cell (Bio-Rad). The membranes were blocked with 5% (w/v) nonfat dried milk in 0.1% (w/v) Tween 20/TBS (T-TBS) for at least 1 h at room temperature, and then incubated with antibodies in the blocking buffer at 4 °C overnight. After washing three times with T-TBS, the membranes were incubated with peroxidase-coupled secondary antibodies in the blocking buffer at room temperature for 1 h. The membranes were then washed four times with T-TBS and visualized using the ECL chemiluminescence system (GE Healthcare).

Assay for cell retraction and detachment following EGTA treatment. Cells were detached from dishes with PBS containing 0.025% trypsin and 1 mM EDTA, washed with DMEM, 0.5% BSA, 10 mM HEPES-NaOH, pH 7.5, and resuspended in the same medium. Cells were plated on 12-well plates coated with 5 nM laminin-511 and cultured for 2h30min. After washing twice with PBS and then once with PBS, 1 mM EGTA, 1 mg/ml glucose containing an inhibitor (Y-27632, blebbistatin or dynasore), cells were treated with the same saline containing the inhibitor at 37 °C for 15 min. Cells were fixed with 3.7% formaldehyde in PBS for 20 min at room temperature and then stained with 0.1% toluidine blue. Stained cells were photographed under a bright-field microscope (Olympus). To quantify the amounts of cells remaining on substrates, the dye in the stained cells was extracted with 0.5% (w/v) SDS and then subjected to colorimetric measurement at 595 nm.

Immunofluorescence staining. A549 cells suspended in DMEM, 0.5% BSA, 10 mM HEPES-NaOH, pH 7.4 were plated on glass coverslips coated with 10 nM laminin-511. For immunostaining of SAMs, cells were cultured for 2h30min after plating. After washing twice with PBS and then once with PBS, 1 mM EGTA, 1 mg/ml glucose, cells were treated with the same saline containing EGTA at 37 °C for 15 min, and then fixed with 3.7% formaldehyde in PBS. For immunostaining of migrating cells, cells were cultured for 1 h after plating and the medium was then changed to DMEM, 1% FBS, 10 mM HEPES-NaOH, pH 7.4. Two hours after the medium change, cells were fixed with 3.7% formaldehyde in PBS. After fixation, cells were permeabilized with 0.2% Brij 97 for 3 min and blocked with PBS containing 2.5% (w/v) BSA. Cells were then incubated with anti-CD9, anti-CD81, or anti-CD151 mouse mAb at 4 °C overnight, followed by washing 3 times with PBS and then incubation with Alexa 488-conjugated anti-mouse IgG antibody at room temperature for 1 h. Actin filaments were stained with rhodamine-conjugated phalloidin. Stained cells were observed under a fluorescent microscope (Axiovert 200, Zeiss).

Time-lapse microscopy. A549 cells suspended in DMEM, 0.5% BSA, 10 mM HEPES-NaOH, pH 7.4 were replated on 35-mm glass-bottom dishes coated with either laminin-511 (10 nM) or type I collagen (300 μg/ml). One hour after plating, the medium was changed to DMEM, 1% FBS, 10 mM HEPES-NaOH, pH 7.4. Two hours after the medium change, cell migration was monitored using an Axiovert 200 inverted microscope (Zeiss). Video images were collected with a CoolSNAP HQ CCD camera (Photometrics) at 30 sec intervals for 30 min using SlideBook software (Intelligent Imaging Innovations).

Scanning electron microscopy. A549 cells suspended in DMEM, 0.5% BSA, 10 mM HEPES-NaOH, pH 7.4 were replated on 35-mm dishes coated with either laminin-511 (5 nM)

or type I collagen (300 μg/ml), and cultured for 2h30min. After washing twice with PBS and then once with PBS, 1 mM EGTA, 1 mg/ml glucose, cells were treated with the same saline containing EGTA at 37 °C for 15 min, and then fixed with 2% glutaraldehyde in 0.1 M sodium phosphate buffer (pH 7.4) at 4 °C. The cells were postfixed in 2% osmium tetroxide solution at 4 °C. The samples were dehydrated in a series of ethanol, immersed in *tert*-butyl alcohol, freeze-dried, and coated with osmium. The samples were examined with a scanning electron microscope (JSM-6320F, JEOL).

Disclosure of Potential Conflicts of Interest

No potential conflicts of interest were disclosed.

Acknowledgments

We thank Noriko Sanzen for establishing hybridoma clones for laminins and CD151 and purifying the mAbs, and Keita Kawamura for assistance in the proteomic analyses. This work was supported by Grants-in-Aid for Scientific Research from the Japan Society for Promotion of Science (to MY and KS) and for Scientific Research on Priority Areas from the Ministry of Education, Culture, Sports, Science and Technology of Japan (to KS).

Supplemental Material

Supplemental materials may be found here:
www.landesbioscience.com/journals/celladhesion/article/25041

References

1. Hynes RO. Integrins: bidirectional, allosteric signaling machines. Cell 2002; 110:673-87; PMID:12297042; http://dx.doi.org/10.1016/S0092-8674(02)00971-6
2. Harburger DS, Calderwood DA. Integrin signalling at a glance. J Cell Sci 2009; 122:159-63; PMID:19118207; http://dx.doi.org/10.1242/jcs.018093
3. Geiger B, Yamada KM. Molecular architecture and function of matrix adhesions. Cold Spring Harb Perspect Biol 2011; 3:a005033; PMID:21441590; http://dx.doi.org/10.1101/cshperspect.a005033
4. Guo W, Giancotti FG. Integrin signalling during tumour progression. Nat Rev Mol Cell Biol 2004; 5:816-26; PMID:15459662; http://dx.doi.org/10.1038/nrm1490
5. Evans R, Patzak I, Svensson L, De Filippo K, Jones K, McDowall A, et al. Integrins in immunity. J Cell Sci 2009; 122:215-25; PMID:19118214; http://dx.doi.org/10.1242/jcs.019117
6. Wickström SA, Radovanac K, Fässler R. Genetic analyses of integrin signaling. Cold Spring Harb Perspect Biol 2011; 3:a005116; PMID:21421914; http://dx.doi.org/10.1101/cshperspect.a005116
7. Huttenlocher A, Horwitz AR. Integrins in cell migration. Cold Spring Harb Perspect Biol 2011; 3:a005074; PMID:21885598; http://dx.doi.org/10.1101/cshperspect.a005074
8. Broussard JA, Webb DJ, Kaverina I. Asymmetric focal adhesion disassembly in motile cells. Curr Opin Cell Biol 2008; 20:85-90; PMID:18083360; http://dx.doi.org/10.1016/j.ceb.2007.10.009
9. Terry AH, Culp LA. Substrate-attached glycoproteins from normal and virus-transformed cells. Biochemistry 1974; 13:414-25; PMID:4358946; http://dx.doi.org/10.1021/bi00700a004
10. Rosen JJ, Culp LA. Morphology and cellular origins of substrate-attached material from mouse fibroblasts. Exp Cell Res 1977; 107:139-49; PMID:405231; http://dx.doi.org/10.1016/0014-4827(77)90395-0
11. Domen C, Culp LA. Adhesion sites of neural tumor cells. Morphogenesis of substratum-attached material. Exp Cell Res 1981; 134:329-38; PMID:6791949; http://dx.doi.org/10.1016/0014-4827(81)90433-X
12. Murray BA, Culp LA. Multiple and masked pools of fibronectin in murine fibroblast cell--substratum adhesion sites. Exp Cell Res 1981; 131:237-49; PMID:7009172; http://dx.doi.org/10.1016/0014-4827(81)90229-9
13. Culp LA, Murray BA, Rollins BJ. Fibronectin and proteoglycans as determinants of cell-substratum adhesion. J Supramol Struct 1979; 11:401-27; PMID:232521; http://dx.doi.org/10.1002/jss.400110314
14. Rollins BJ, Culp LA. Glycosaminoglycans in the substrate adhesion sites of normal and virus-transformed murine cells. Biochemistry 1979; 18:141-8; PMID:217403; http://dx.doi.org/10.1021/bi00568a022
15. Mugnai G, Tombaccini D, Ruggieri S. Ganglioside composition of substrate-adhesion sites of normal and virally-transformed Balb/c 3T3 cells. Biochem Biophys Res Commun 1984; 125:142-8; PMID:6508793; http://dx.doi.org/10.1016/S0006-291X(84)80346-0
16. Barletta E, Mugnai G, Ruggieri S. Morphological characteristics and ganglioside composition of substratum adhesion sites in a hepatoma cell line (CMH5123 cells) during different phases of growth. Exp Cell Res 1989; 182:394-402; PMID:2498113; http://dx.doi.org/10.1016/0014-4827(89)90244-9
17. Peñas PF, García-Díez A, Sánchez-Madrid F, Yáñez-Mó M. Tetraspanins are localized at motility-related structures and involved in normal human keratinocyte wound healing migration. J Invest Dermatol 2000; 114:1126-35; PMID:10844555; http://dx.doi.org/10.1046/j.1523-1747.2000.00998.x
18. Zhang XA, Huang C. Tetraspanins and cell membrane tubular structures. Cell Mol Life Sci 2012; 69:2843-52; PMID:22450717; http://dx.doi.org/10.1007/s00018-012-0954-0
19. Vicente-Manzanares M, Ma X, Adelstein RS, Horwitz AR. Non-muscle myosin II takes centre stage in cell adhesion and migration. Nat Rev Mol Cell Biol 2009; 10:778-90; PMID:19851336; http://dx.doi.org/10.1038/nrm2786
20. Ezratty EJ, Partridge MA, Gundersen GG. Microtubule-induced focal adhesion disassembly is mediated by dynamin and focal adhesion kinase. Nat Cell Biol 2005; 7:581-90; PMID:15895076; http://dx.doi.org/10.1038/ncb1262
21. Hemler ME. Tetraspanin functions and associated microdomains. Nat Rev Mol Cell Biol 2005; 6:801-11; PMID:16314869; http://dx.doi.org/10.1038/nrm1736
22. Charrin S, le Naour F, Silvie O, Milhiet PE, Boucheix C, Rubinstein E. Lateral organization of membrane proteins: tetraspanins spin their web. Biochem J 2009; 420:133-54; PMID:19426143; http://dx.doi.org/10.1042/BJ20082422
23. Yáñez-Mó M, Barreiro O, Gordon-Alonso M, Sala-Valdés M, Sánchez-Madrid F. Tetraspanin-enriched microdomains: a functional unit in cell plasma membranes. Trends Cell Biol 2009; 19:434-46; PMID:19709882; http://dx.doi.org/10.1016/j.tcb.2009.06.004
24. André M, Le Caer JP, Greco C, Planchon S, El Nemer W, Boucheix C, et al. Proteomic analysis of the tetraspanin web using LC-ESI-MS/MS and MALDI-FTICR-MS. Proteomics 2006; 6:1437-49; PMID:16404722; http://dx.doi.org/10.1002/pmic.200500180
25. Palecek SP, Schmidt CE, Lauffenburger DA, Horwitz AF. Integrin dynamics on the tail region of migrating fibroblasts. J Cell Sci 1996; 109:941-52; PMID:8743941
26. Rigort A, Grünewald J, Herzog V, Kirfel G. Release of integrin macroaggregates as a mechanism of rear detachment during keratinocyte migration. Eur J Cell Biol 2004; 83:725-33; PMID:15679117; http://dx.doi.org/10.1078/0171-9335-00431
27. Kirfel G, Rigort A, Borm B, Schulte C, Herzog V. Structural and compositional analysis of the keratinocyte migration track. Cell Motil Cytoskeleton 2003; 55:1-13; PMID:12673594; http://dx.doi.org/10.1002/cm.10106
28. Chao WT, Kunz J. Focal adhesion disassembly requires clathrin-dependent endocytosis of integrins. FEBS Lett 2009; 583:1337-43; PMID:19306879; http://dx.doi.org/10.1016/j.febslet.2009.03.037
29. Ezratty EJ, Bertaux C, Marcantonio EE, Gundersen GG. Clathrin mediates integrin endocytosis for focal adhesion disassembly in migrating cells. J Cell Biol 2009; 187:733-47; PMID:19951918; http://dx.doi.org/10.1083/jcb.200904054
30. Macia E, Ehrlich M, Massol R, Boucrot E, Brunner C, Kirchhausen T. Dynasore, a cell-permeable inhibitor of dynamin. Dev Cell 2006; 10:839-50; PMID:16740485; http://dx.doi.org/10.1016/j.devcel.2006.04.002
31. Kirfel G, Rigort A, Borm B, Herzog V. Cell migration: mechanisms of rear detachment and the formation of migration tracks. Eur J Cell Biol 2004; 83:717-24; PMID:15679116; http://dx.doi.org/10.1078/0171-9335-00421
32. Worthylake RA, Lemoine S, Watson JM, Burridge K. RhoA is required for monocyte tail retraction during transendothelial migration. J Cell Biol 2001; 154:147-60; PMID:11448997; http://dx.doi.org/10.1083/jcb.200103048
33. Vicente-Manzanares M, Zareno J, Whitmore L, Choi CK, Horwitz AF. Regulation of protrusion, adhesion dynamics, and polarity by myosins IIA and IIB in migrating cells. J Cell Biol 2007; 176:573-80; PMID:17312025; http://dx.doi.org/10.1083/jcb.200612043
34. Lawson MA, Maxfield FR. Ca(2+)- and calcineurin-dependent recycling of an integrin to the front of migrating neutrophils. Nature 1995; 377:75-9; PMID:7544874; http://dx.doi.org/10.1038/377075a0
35. Stipp CS. Laminin-binding integrins and their tetraspanin partners as potential antimetastatic targets. Expert Rev Mol Med 2010; 12:e3; PMID:20078909; http://dx.doi.org/10.1017/S1462399409001355
36. Richardson MM, Jennings LK, Zhang XA. Tetraspanins and tumor progression. Clin Exp Metastasis 2011; 28:261-70; PMID:21184145; http://dx.doi.org/10.1007/s10585-010-9365-5
37. Romanska HM, Berditchevski F. Tetraspanins in human epithelial malignancies. J Pathol 2011; 223:4-14; PMID:20938929; http://dx.doi.org/10.1002/path.2779

38. Zöller M. Tetraspanins: push and pull in suppressing and promoting metastasis. Nat Rev Cancer 2009; 9:40-55; PMID:19078974; http://dx.doi.org/10.1038/nrc2543
39. Zijlstra A, Lewis J, Degryse B, Stuhlmann H, Quigley JP. The inhibition of tumor cell intravasation and subsequent metastasis via regulation of in vivo tumor cell motility by the tetraspanin CD151. Cancer Cell 2008; 13:221-34; PMID:18328426; http://dx.doi.org/10.1016/j.ccr.2008.01.031
40. Thorne RF, Mhaidat NM, Ralston KJ, Burns GF. Shed gangliosides provide detergent-independent evidence for type-3 glycosynapses. Biochem Biophys Res Commun 2007; 356:306-11; PMID:17350595; http://dx.doi.org/10.1016/j.bbrc.2007.02.139
41. Todeschini AR, Dos Santos JN, Handa K, Hakomori SI. Ganglioside GM2-tetraspanin CD82 complex inhibits met and its cross-talk with integrins, providing a basis for control of cell motility through glycosynapse. J Biol Chem 2007; 282:8123-33; PMID:17215249; http://dx.doi.org/10.1074/jbc.M611407200
42. Odintsova E, Butters TD, Monti E, Sprong H, van Meer G, Berditchevski F. Gangliosides play an important role in the organization of CD82-enriched microdomains. Biochem J 2006; 400:315-25; PMID:16859490; http://dx.doi.org/10.1042/BJ20060259
43. Ono M, Handa K, Sonnino S, Withers DA, Nagai H, Hakomori S. GM3 ganglioside inhibits CD9-facilitated haptotactic cell motility: coexpression of GM3 and CD9 is essential in the downregulation of tumor cell motility and malignancy. Biochemistry 2001; 40:6414-21; PMID:11371204; http://dx.doi.org/10.1021/bi0101998
44. Mitsuzuka K, Handa K, Satoh M, Arai Y, Hakomori S. A specific microdomain ("glycosynapse 3") controls phenotypic conversion and reversion of bladder cancer cells through GM3-mediated interaction of α3β1 integrin with CD9. J Biol Chem 2005; 280:35545-53; PMID:16103120; http://dx.doi.org/10.1074/jbc.M505630200
45. Hakomori SI. Glycosynaptic microdomains controlling tumor cell phenotype through alteration of cell growth, adhesion, and motility. FEBS Lett 2010; 584:1901-6; PMID:19874824; http://dx.doi.org/10.1016/j.febslet.2009.10.065
46. Cramer LP. Forming the cell rear first: breaking cell symmetry to trigger directed cell migration. Nat Cell Biol 2010; 12:628-32; PMID:20596043; http://dx.doi.org/10.1038/ncb0710-628
47. Yamada M, Sumida Y, Fujibayashi A, Fukaguchi K, Sanzen N, Nishiuchi R, et al. The tetraspanin CD151 regulates cell morphology and intracellular signaling on laminin-511. FEBS J 2008; 275:3335-51; PMID:18492066; http://dx.doi.org/10.1111/j.1742-4658.2008.06481.x
48. Nishiuchi R, Sanzen N, Nada S, Sumida Y, Wada Y, Okada M, et al. Potentiation of the ligand-binding activity of integrin α3β1 via association with tetraspanin CD151. Proc Natl Acad Sci U S A 2005; 102:1939-44; PMID:15677332; http://dx.doi.org/10.1073/pnas.0409493102
49. Boucheix C, Rubinstein E. Tetraspanins. Cell Mol Life Sci 2001; 58:1189-205; PMID:11577978; http://dx.doi.org/10.1007/PL00000933
50. Berditchevski F. Complexes of tetraspanins with integrins: more than meets the eye. J Cell Sci 2001; 114:4143-51; PMID:11739647
51. Le Naour F, André M, Boucheix C, Rubinstein E. Membrane microdomains and proteomics: lessons from tetraspanin microdomains and comparison with lipid rafts. Proteomics 2006; 6:6447-54; PMID:17109380; http://dx.doi.org/10.1002/pmic.200600282
52. Tarrant JM, Robb L, van Spriel AB, Wright MD. Tetraspanins: molecular organisers of the leukocyte surface. Trends Immunol 2003; 24:610-7; PMID:14596886; http://dx.doi.org/10.1016/j.it.2003.09.011
53. Kovalenko OV, Yang XH, Hemler ME. A novel cysteine cross-linking method reveals a direct association between claudin-1 and tetraspanin CD9. Mol Cell Proteomics 2007; 6:1855-67; PMID:17644758; http://dx.doi.org/10.1074/mcp.M700183-MCP200
54. Chattopadhyay N, Wang Z, Ashman LK, Brady-Kalnay SM, Kreidberg JA. α3β1 integrin-CD151, a component of the cadherin-catenin complex, regulates PTPmu expression and cell-cell adhesion. J Cell Biol 2003; 163:1351-62; PMID:14691142; http://dx.doi.org/10.1083/jcb.200306067
55. Yañez-Mó M, Barreiro O, Gonzalo P, Batista A, Megías D, Genís L, et al. MT1-MMP collagenolytic activity is regulated through association with tetraspanin CD151 in primary endothelial cells. Blood 2008; 112:3217-26; PMID:18663148; http://dx.doi.org/10.1182/blood-2008-02-139394
56. Lafleur MA, Xu D, Hemler ME. Tetraspanin proteins regulate membrane type-1 matrix metalloproteinase-dependent pericellular proteolysis. Mol Biol Cell 2009; 20:2030-40; PMID:19211836; http://dx.doi.org/10.1091/mbc.E08-11-1149
57. Wakabayashi T, Craessaerts K, Bammens L, Bentahir M, Borgions F, Herdewijn P, et al. Analysis of the gamma-secretase interactome and validation of its association with tetraspanin-enriched microdomains. Nat Cell Biol 2009; 11:1340-6; PMID:19838174; http://dx.doi.org/10.1038/ncb1978
58. Domínguez F, Simón C, Quiñonero A, Ramírez MA, González-Muñoz E, Burghardt H, et al. Human endometrial CD98 is essential for blastocyst adhesion. PLoS One 2010; 5:e13380; PMID:20976164; http://dx.doi.org/10.1371/journal.pone.0013380
59. Dornier E, Coumailleau F, Ottavi JF, Moretti J, Boucheix C, Mauduit P, et al. TspanC8 tetraspanins regulate ADAM10/Kuzbanian trafficking and promote Notch activation in flies and mammals. J Cell Biol 2012; 199:481-96; PMID:23091066; http://dx.doi.org/10.1083/jcb.201201133
60. Gilsanz A, Sánchez-Martín L, Gutiérrez-López MD, Ovalle S, Machado-Pineda Y, Reyes R, et al. ALCAM/CD166 adhesive function is regulated by the tetraspanin CD9. Cell Mol Life Sci 2013; 70:475-93; PMID:23052204; http://dx.doi.org/10.1007/s00018-012-1132-0
61. Berditchevski F, Chang S, Bodorova J, Hemler ME. Generation of monoclonal antibodies to integrin-associated proteins. Evidence that α3β1 complexes with EMMPRIN/basigin/OX47/M6. J Biol Chem 1997; 272:29174-80; PMID:9360995; http://dx.doi.org/10.1074/jbc.272.46.29174
62. Merlin D, Sitaraman S, Liu X, Eastburn K, Sun J, Kucharzik T, et al. CD98-mediated links between amino acid transport and beta 1 integrin distribution in polarized columnar epithelia. J Biol Chem 2001; 276:39282-9; PMID:11507094; http://dx.doi.org/10.1074/jbc.M105077200
63. Rintoul RC, Buttery RC, Mackinnon AC, Wong WS, Mosher D, Haslett C, et al. Cross-linking CD98 promotes integrin-like signaling and anchorage-independent growth. Mol Biol Cell 2002; 13:2841-52; PMID:12181350; http://dx.doi.org/10.1091/mbc.01-11-0530

IJC
International Journal of Cancer

New findings of kinase switching in gastrointestinal stromal tumor under imatinib using phosphoproteomic analysis

Tsuyoshi Takahashi[1,2], Satoshi Serada[2], Maiko Ako[2], Minoru Fujimoto[2], Yasuaki Miyazaki[1], Rie Nakatsuka[1,2], Takayuki Ikezoe[3], Akihito Yokoyama[3], Takahiro Taguchi[4], Kazuki Shimada[5], Yukinori Kurokawa[1], Makoto Yamasaki[1], Hiroshi Miyata[1], Kiyokazu Nakajima[1], Shuji Takiguchi[1], Masaki Mori[1], Yuichiro Doki[1], Tetsuji Naka[2] and Toshirou Nishida[2,6]

[1] Department of Surgery, Osaka University Graduate School of Medicine, Suita, Japan
[2] Laboratory for Immune Signal, National Institute of Biomedical Innovation, Ibaraki, Japan
[3] Department of Hematology and Respiratory Medicine, Kochi Medical School, Kochi University, Nankoku, Japan
[4] Research and Education Faculty, Multidisciplinary Science Cluster, Kuroshio Science Unit, Kochi Medical School, Kochi University, Nankoku, Japan
[5] Department of Respiratory Medicine, Allergy and Rheumatic Diseases, Osaka University Graduate School of Medicine, Suita, Japan
[6] Department of Surgery, Osaka Police Hospital, Osaka, Japan

Despite the revolutionary effects of imatinib on advanced gastrointestinal stromal tumors (GISTs), most patients eventually develop disease progression following primary resistance or acquired resistance driven by secondary-resistant mutations. Even in radiographically vanishing lesions, pathology has revealed persistent viable cells during imatinib therapy, which could lead to the emergence of drug-resistant clones. To uncover the mechanisms underlying these clinical issues, here we examined imatinib-induced phosphoproteomic alterations in GIST-T1 cells, using our quantitative tyrosine phosphoproteomic analysis method, which combined immunoaffinity enrichment of phosphotyrosine-containing peptides with isobaric tags for relative and absolute quantitation (iTRAQ) technology. Using this approach, we identified 171 tyrosine phosphorylation sites spanning 134 proteins, with 11 proteins exhibiting greater than 1.5-fold increases in tyrosine phosphorylation. Among them, we evaluated FYN and focal adhesion kinase (FAK), both of which are reportedly involved in proliferation and malignant alteration of tumors. We confirmed increased tyrosine phosphorylation of both kinases by western blotting. Inhibition of FYN and FAK phosphorylation each increased tumor cell sensitivity to imatinib. Furthermore, a FAK-selective inhibitor (TAG372) induced apoptosis of imatinib-resistant GIST-T1 cells and decreased the imatinib IC_{50}. These results indicate that FYN or FAK might be potential therapeutic targets to overcome resistance to imatinib in GISTs. Additionally, we showed that the iTRAQ-based quantitative phosphotyrosine-focused phosphoproteomic approach is a powerful method for screening phosphoproteins associated with drug resistance.

The gastrointestinal stromal tumor (GIST) is the most common mesenchymal tumor of the digestive tract, and is characterized by expression of the KIT (CD117) and/or DOG1 proteins. Most GISTs have oncogenic *KIT* or *PDFGRA* mutations, which is a key factor in sporadic GIST pathogenesis and proliferation.[1–3] This knowledge has facilitated the development of targeted therapies with tyrosine kinase inhibitors and led to the revolutionary treatment with imatinib mesylate (Glivec®; Novartis Pharmaceuticals). Recent clinical trials with advanced/unresectable GIST have shown that imatinib produces objective responses in ~50% of patients, and disease stabilization (stable disease) in another 30–40%. The corresponding 2-year overall survival rates range from 70 to 80%, indicating markedly improved patient outcomes compared with anecdotal data from cytotoxic chemotherapy in the preimatinib era.[4–6]

Despite imatinib's effectiveness, there remain several problems. First, GIST patients cannot stop taking the drug even if complete response is obtained, because discontinuation inevitably leads to reprogression and disease relapse.[7,8] Second, imatinib activity is limited by primary resistance to the drug in ~15% of patients, and secondary resistance eventually develops in more than 80% of patients.[5,9] Secondary resistance mainly occurs due to additional kinase domain mutations, which are thought to develop in viable tumor cells (persistent cells) during imatinib therapy. It is not yet known

Key words: GIST, imatinib, iTRAQ, proteomics

Abbreviations: FAK: focal adhesion kinase; GIST: gastrointestinal stromal tumor; iTRAQ: isobaric tags for relative and absolute quantitation; LC: liquid chromatography; MS/MS: tandem mass spectrometry; shRNA: small hairpin RNA; siRNA: small interfering RNA

Additional Supporting Information may be found in the online version of this article.

DOI: 10.1002/ijc.28282
History: Received 17 Dec 2012; Accepted 2 May 2013; Online 28 May 2013

Correspondence to: Toshirou Nishida, Department of Surgery, Osaka Police Hospital, 10-31, Kitayama-cho, Tennoji-ku, Osaka 543-0035, Japan, Tel.: +81-6-6771-6051, Fax: +81-6-6775-2838, E-mail: toshin@mvb.biglobe.ne.jp

Short Report

What's new?
While the targeted tyrosine kinase inhibitor imatinib can significantly improve two-year survival rates for patients with gastrointestinal stromal tumor (GIST), primary and secondary resistance mutations often limit its benefits. This study of the human GIST-T1 cell line suggests that imatinib-induced increases in tyrosine phosphorylation of FYN kinase and focal adhesion kinase (FAK) may be responsible for mediating some instances of imatinib resistance and therefore may be potential targets for killing persistent tumor cells and overcoming resistance. The findings also indicate that iTRAQ-based quantitative phosphotyrosine-focused proteomic analysis is a useful way of screening for phosphoproteins associated with drug resistance.

what mechanisms keep these persistent cells alive after shutdown of KIT signaling by imatinib.

Phosphorylation of protein kinases in signaling pathways is a key event in tumor cell survival and proliferation. Differential phosphoprotein analysis may provide clues to alternatively activated pathways and/or substituted kinases that may be activated after inhibition of main pathways, such as KIT.[10] Recent advances in mass spectrometry-based phosphoproteomics enable extensive profiling of serine-threonine kinases, while tyrosine kinase analysis has remained challenging in terms of quantity and quality. However, a recent method coupling peptide-level antiphosphotyrosine immunoaffinity purification with liquid chromatography (LC)-tandem mass spectrometry (MS/MS) has provided reasonable profiling for tyrosine phosphorylation.[11]

In the present study, we quantitatively measured the phosphoproteomic alterations induced by imatinib in a GIST-T1 cell line. We also examined the roles of some tyrosine kinases that were activated in persistent tumor cells after imatinib exposure.

Material and Methods

Cell lines

We previously established the human GIST cell line GIST-T1, which has a 57-nucleotide (V570-Y578) in-frame deletion in KIT exon 11.[12] The cell line identity was confirmed by DNA fingerprinting through short tandem repeat profiling, as previously described.[13] GIST-T1-R was established from GIST-T1 as an imatinib-resistant clone that arose from continuous culturing in 5 μM imatinib. The GIST-T1-R cells GIST-T1-R2 and GIST-T1-R8 each exhibit imatinib IC_{50} values of ~30 μM, which is ~1000 times that of the GIST-T1 parent.

Reagents and antibodies

Imatinib and TAG372—selective tyrosine kinase inhibitors for KIT and focal adhesion kinase (FAK), respectively—were synthesized and provided by Novartis Pharmaceuticals (Basel, Switzerland). The following primary antibodies were used: anti-phospho-Src Family (Tyr416) (1:1000), anti-phospho-ERK and anti-ERK from Cell Signaling Technology (Danvers, MA); anti-GAPDH from Santa Cruz Biotechnology (Santa Cruz, CA); anti-phospho-FAK (Tyr397) from Biosource (Camarillo, CA); anti-FAK from BD Transduction Laboratories (San Jose, CA) and anti-phosphotyrosine (clone 4G10) from Upstate Biotechnology (Lake Placid, NY). Detailed immunoprecipitation information is provided in the Supporting Information Materials and Methods section.

Peptide synthesis

A tyrosine-phosphorylated peptide (NVPLyK) derived from a trypsinized peptide sequence of yeast alpha-enolase was synthesized at Sigma Aldrich (Milwaukee, WI) using standard solid-phase peptide synthesis techniques and Fmoc chemistry.

Phosphopeptide immunoprecipitation

GIST-T1 cells were treated with 400 nM of imatinib for 0, 1, 6 and 24 hr. Tyrosine-phosphorylated peptides were purified using Cell Signaling PhosphoScan pTyr100 Kits (Beverly, MA) following the manufacturer's instructions with minor modification. Detailed information is provided in the Supporting Information Materials and Methods section.

iTRAQ labeling

After immunoprecipitation, peptides were dissolved in 9.8 M Urea (5 μL) and 1 M TEAB (20 μL). Following the manufacturer's protocol (Applied Biosystems, Foster City, CA), the samples were labeled with the isobaric tags for relative and absolute quantitation (iTRAQ) reagents as follows: GIST-T1 with reagent 114 (0 hr), GIST-T1 with reagent 115 (1 hr), GIST-T1 with reagent 116 (6 hr) and GIST-T1 with reagent 117 (24 hr). The labeled peptide samples were then pooled and desalted with Sep-Pak Light C18 Cartridges, and the peptides were dried in a SpeedVac. The labeled peptide mixtures were purified and fractionated into 14 fractions using strong cation exchange fractionation, as previously described.[13]

Quantitative mass spectrometric analysis

Nano LC-MS/MS analysis and iTRAQ data analysis were performed as described in the Supporting Information Materials and Methods section.

Small interfering RNA transfection

Commercial FAK small interfering RNA (siRNA) and nonspecific siRNA were obtained from QIAGEN. Cells were transfected with siRNA using Lipofectamine 2000 reagent

(Invitrogen) following the manufacturer's instructions. Selective silencing of FAK was confirmed by western blot analysis.

Generation of FYN knockdown cells

To generate stable FYN knockdown cell lines, GIST-T1 cells were transfected with a commercial plasmid containing an anti-FYN short hairpin RNA (shRNA Fyn, plasmid KH00147N; SABiosciences [Qiagen], Frederick, MD) using Lipofectamine 2000 (Invitrogen, Carlsbad, CA) according to the manufacturer's instructions. The correctly transfected and expressing cells were selected with 600 μg/mL G418 (Invitrogen). Stable clones were maintained in 250 μg/mL G418. Three stable GIST-T1-FYN shRNA cell lines were established, designated B1, B2 and B3 cells. We also established a control cell line of GIST-T1 stably transfected with the empty vector, which we designated GIST-T1-C.

Measurement of IC_{50} after imatinib treatment

Cells were seeded in 96-well plates at 2000 cells/well (Costar; Corning, Corning, NY) for 24 hr and then exposed to various concentrations (0–40 μM) of imatinib for 72 hr. Cell proliferation was evaluated with the WST-8 [2-(2-methoxy-4-nitrophenyl)-3-(4-nitrophenyl)-5-(2,4-disulfophenyl)-2H-tetrazolium, monosodium salt] assay (Cell Counting Kit-SF; Nacalai Tesque) at the indicated post-treatment times. A microplate reader Model 680 (Bio-Rad Laboratories, Hercules, CA) was used to measure WST-8 absorption at a wavelength of 450 nm with a reference wavelength of 630 nm. Growth rate was expressed as the percentage of absorbance for treated cells vs. control cells. Experiments were performed in triplicate in two independent experiments, and the presented values are the averages of all six wells.

Apoptosis assay

GIST-T1 cells were seeded in 6-well plates at a density of 3×10^5 cells per well and treated with imatinib and/or TAG372 for 2 days. The cells were then washed with PBS, and caspase-3 activity was detected using the caspase-3 fluorometric assay kit (R&D systems, Minneapolis, MN) following the manufacturer's instructions. The presented values are the means of three independent experiments.

Statistical analysis

Statistical analyses were performed using the Mann–Whitney *U*-test or one-way analysis of variance (ANOVA), followed by Scheffe's test. One-way ANOVA followed by Dunnett's test was used for multiple comparisons.

Results

Quantitative phosphotyrosine proteomic analysis identifies upregulation of FYN and FAK in imatinib-exposed GIST-T1 cells

GIST-T1 cells that possessed the activating mutation in exon 11 of *KIT* are sensitive to imatinib, with a K_i value for imatinib of 20 nM. Time-dependent decreases in the tyrosine phosphorylation of KIT were observed when GIST-T1 cells were treated with 400 nM imatinib for 0, 1, 6 and 24 hr (Fig. 1*a*). These time-points were used for subsequent MS analysis, with 0 hr used as a control.

By utilizing immunoaffinity enrichment of phosphotyrosine peptides with quantitative phosphoproteomic analysis using iTRAQ technology combined with nano LC-MS/MS analysis, we identified 171 tyrosine phosphorylation sites spanning 134 proteins (Supporting Information Table S1). After imatinib treatment, a total of 11 phosphotyrosine sites spanning 11 proteins exhibited increases of >1.5-fold and 21 phosphotyrosine sites spanning 15 proteins showed decreases of <0.3-fold (Table 1). As a representative protein, we confirmed a dramatic decrease in the tyrosine phosphorylation levels of the KIT protein (Y609, Y703, Y747, Y823 and Y936). In contrast, imatinib induced increased phosphorylation of FYN (Y420) and FAK (Y576). Phosphorylation of FYN (Y420) upregulates tyrosine kinase activities, and phosphorylation of FAK (Y576) is critical for its maximal catalytic activity.

To validate these results obtained from iTRAQ analysis, we further examined the tyrosine phosphorylation of FYN and FAK using western blotting. As shown in iTRAQ analysis, western blotting confirmed that FYN (Y420) and FAK (Y576) were time dependently phosphorylated (Figs. 1*b* and 2*c*). When tyrosine phosphorylation in the activation loop was measured for other Src family kinases, we found that imatinib treatment did not increase tyrosine phosphorylation of SRC, LYN, LCK or YES (Fig. 1*b*).

Inhibition of FYN or FAK enhances imatinib sensitivity of GIST-T1 cells

To examine the functions of FYN in GIST-T1 cells exposed to imatinib, FYN expression was stably suppressed using a FYN shRNA plasmid. We cloned and established GIST-T1 B1, B2 and B3 cells, as well as GIST-T1 C cells transfected with empty vector as a control (Fig. 1*d*). Compared with GIST-T1 C cells, the FYN knockdown cell lines showed significantly decreased IC_{50} values for imatinib ($p < 0.05$; Fig. 1*d*).

We also examined the role of FAK activation in imatinib treatment. We repressed FAK expression using siRNA, and we used a FAK inhibitor (TAG372) to inhibit FAK phosphorylation. Transfection of FAK siRNA reduced IC_{50} values for imatinib ($p < 0.05$; Fig. 1*e*). When used with imatinib, TAG372 further decreased cell survival in a dose-dependent manner (Fig. 1*f*).

Inhibition of FAK improves imatinib sensitivity in GIST-T1-R cells

Next, we examined FAK activation in imatinib-resistant cell lines established from GIST-T1 cells. Eight imatinib-resistant cell lines were established by incubation of GIST-T1 cells with imatinib of gradually increased concentrations. Constitutive phosphorylation of FAK was observed in two imatinib-resistant

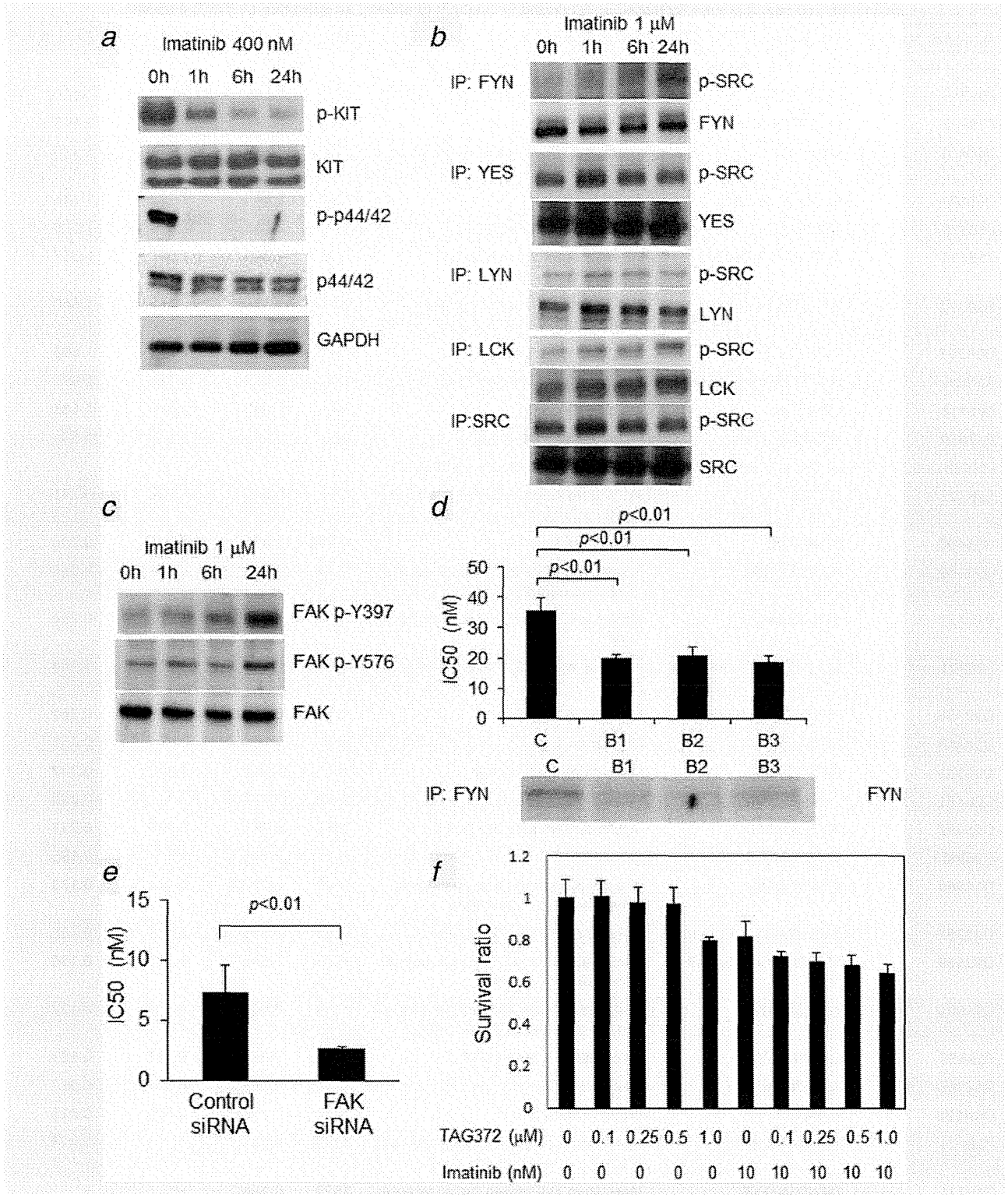

Figure 1. (*a*) Altered tyrosine phosphorylation levels detected by iTRAQ analysis were confirmed by western blotting. Imatinib treatment led to reduced phosphotyrosine levels. (*b*) Imatinib treatment changed SRC family kinase phosphorylation levels. (*c*) iTRAQ analysis showed that FYN (Y420) and FAK (Y576) exhibited similar tyrosine phosphorylation. (*d*) Compared with in GIST-T1 C cells, the IC_{50} for imatinib was significantly reduced in all FYN knockdown GIST-T1 cells (B1, B2 and B3). (*e*) The IC_{50} for imatinib was reduced in GIST-T1 cells that were transfected with FAK siRNA. (*f*) WST-8 assay showed the cell viability with imatinib and TAG372 treatment. Data are presented as means ± SD.

Table 1. Phosphotyrosine peptides that were increased or decreased by imatinib treatment, as quantified by iTRAQ analysis[1]

Accession Number	Sequence	Description	Site	1 hr/0 hr[2]	6 hr/0 hr[2]	24 hr/0 hr[2]
Greater than 1.5-fold increase of phosphorylated peptide at 24 hr compared with 0 hr						
P06241	LIEDNEYTAR	Tyrosine-protein kinase Fyn	Y420	0.845	2.365	3.641
P15880	AFVAIGDYNGHVGLGVK	40S ribosomal protein S2	Y133	2.138	1.807	2.443
O00401	VIYDFIEK	Neural Wiskott-Aldrich syndrome protein	Y256	0.768	1.491	1.978
Q99623	MLGEALSKNPGYIK	Prohibitin-2	Y248	1.446	1.778	1.726
P62829	NLYIISVK	60S ribosomal protein L23	Y38	2.138	1.348	1.679
P18433	VVQEYIDAFSDYANFK	Receptor-type tyrosine-protein phosphatase alpha	Y791	1.245	1.098	1.667
P30040	FDTQYPYGEK	Endoplasmic reticulum resident protein 29	Y64	1.804	2.558	1.640
Q05397	YMEDSTYYK	Focal adhesion kinase 1	Y570	1.043	0.893	1.606
A6NI28	LDTASSNGYQRPGSVVAAK	Rho GTPase-activating protein 42	Y792	0.599	0.980	1.594
P08758	LYDAYELK	Annexin A5	Y94	1.043	1.399	1.581
P18669	HYGGLTGLNK	Phosphoglycerate mutase 1	Y92	0.930	2.583	1.532
Less than 0.3-fold reduction of phosphorylated peptide at 24 hr compared with 0 hr						
P10721	IGSYIER	Mast/stem cell growth factor receptor Kit	Y747	0.649	0.244	0.291
O95490	SENEDIYYK	Latrophilin-2	Y1350	0.431	0.318	0.256
Q92569	LQEYHSQYQEK	Phosphatidylinositol 3-kinase regulatory subunit gamma	Y184	0.433	0.271	0.255
P10721	QEDHAEAALYK	Mast/stem cell growth factor receptor Kit	Y703	0.560	0.207	0.254
P10721	QISESTNHIYSNLANCSPNR	Mast/stem cell growth factor receptor Kit	Y936	0.445	0.212	0.244
Q92796	RDNEVDGQDYHFVVSR	Disks large homolog 3	Y673	0.556	0.427	0.241
Q5XXA6	STIVYEILKR	Anoctamin-1	Y251	0.508	0.720	0.235
Q00535	IGEGTYGTVFK	Cyclin-dependent kinase 5	Y15	1.877	0.821	0.232
Q06481	MQNHGYENPTYK	Amyloid-like protein 2	Y755	0.474	–[4]	0.220
O95297	INKSESVVYADIR	Myelin protein zero-like protein 1	Y263	0.785	0.249	0.211
Q969M3	QYAGYDYSQQGR	Protein YIPF5	Y42	0.145	–[4]	0.195
O14964	VVQDTYQIMK	Hepatocyte growth factor-regulated tyrosine kinase substrate	Y132	1.097	0.464	0.173
O95297	SESVVYADIR	Myelin protein zero-like protein 1	Y263	0.563	0.169	0.166
Q92569	VQAEDLLYGKPDGAFLIR	Phosphatidylinositol 3-kinase regulatory subunit gamma	Y373	1.186	0.176	0.130
O96000	YQDLGAYSSAR	NADH dehydrogenase [ubiquinone] 1 beta subcomplex subunit 10	Y143	0.864	0.393	0.122
P16333	LYDLNMPAYVK	Cytoplasmic protein NCK1	Y112	0.651	0.257	0.103
Q12846	NILSSADYVER	Syntaxin-4	Y251	0.179	0.131	0.072
Q8N128	YQYAIDEYYR	Protein FAM177A1	Y162	0.196	0.090	0.055
P10721	VVEATAYGLIK	Mast/stem cell growth factor receptor Kit	Y609	0.723	–[4]	0.023
P10721	DIKNDSNYVVK	Mast/stem cell growth factor receptor Kit	Y823	0.164	–[4]	–[4]
P53778	QADSEMTGYVVTR	Mitogen-activated protein kinase 12	Y185	1.582	0.888	–[4]

[1]The full list is provided in Supporting Information Table 1.
[2]The ratio of peptide derived from the iTRAQ reporter ion, as determined by iTRAQ analysis; 1 hr/0 hr, 6 hr/0 hr and 24 hr/0 hr refer, respectively, to the value of each peptide at 1, 6 and 24 hr divided by the value of that peptide at 0 hr.
[3]A 0-hr value of 0 (*i.e.* below background) and a positive value at 1, 6 or 24 hr.
[4]A 0-hr positive value and a value of 0 (*i.e.* below background) at 1, 6 or 24 hr.

GIST-T1 cell lines (GIST-T1-R2 and GIST-T1-R8), which had imatinib IC_{50} values of 30 μM, ~1000 times that of the GIST-T1 parent cells (Fig. 2*a*). TAG372 dose dependently inhibited FAK phosphorylation in GIST-T1-R2 (Fig. 2*b*), and significantly reduced the imatinib IC_{50} values when both drugs were used (Fig. 2*c*). Moreover, TAG372 induced apoptosis in GIST-T1-R2 (Fig. 2*d*). These results indicate that imatinib treatment induced activation of FYN and FAK in persistent GIST-T1 cells and was associated with imatinib insensitivity and resistance.

Discussion

Imatinib is a selective tyrosine kinase inhibitor of KIT, PDGFRA, ABL/BCR-ABL and CSF-1R, which was first used to treat GIST in 2000. Since then, it has been a standard treatment for advanced and/or recurrent GISTs.[6] Patients with advanced GIST usually respond to imatinib; however, most patients eventually experience disease progression with the reactivation of KIT tyrosine kinase and its downstream signaling pathways.[14,15] Although imatinib has high activity against GISTs, it cannot achieve complete eradication of tumor cells *in vivo* or *in vitro*. Results of the BFR14 trial showed that stopping imatinib treatment, even after complete response, resulted in disease progression or recurrence.[7,8] In chronic myelogenous leukemia (CML), mathematical models have indicated that secondary mutations might emerge after imatinib therapy;[16] therefore, residual tumor cells may also be a predisposing factor for acquired resistance to imatinib in GIST.

To quantitate the alteration of tyrosine phosphorylation levels induced by imatinib, we established quantitative tyrosine phosphoproteomic analysis. Using this technology, we identified 171 different tyrosine phosphorylation sites in 134 proteins of GIST-T1 cells. As we were searching for alternative pathways that were activated after inhibition of KIT signaling by imatinib, we pursued tyrosine kinases with increased tyrosine phosphorylation. Our comprehensive measures indicated that 11 tyrosine kinases exhibited tyrosine phosphorylation increases of greater than 1.5-fold (Table 1). The findings of the phosphoproteomic analysis were confirmed by western blotting showing the tyrosine-phosphorylation of KIT, FAK and other src-family kinases. SRC and LYN are reportedly phosphorylated and activated in GIST after imatinib treatment;[18] however, in the phosphoproteomic and western blotting analyses in the present study, we did not detect activation of SRC, LYN, YES, Lck or any other Src family kinases, except for FYN and FAK. Activation of FYN and FAK is reportedly involved in tumor proliferation and malignant transformation.[17–20]

FYN appears to participate in cell growth and survival, acting downstream of integrin and PI3K.[17,21] Although the

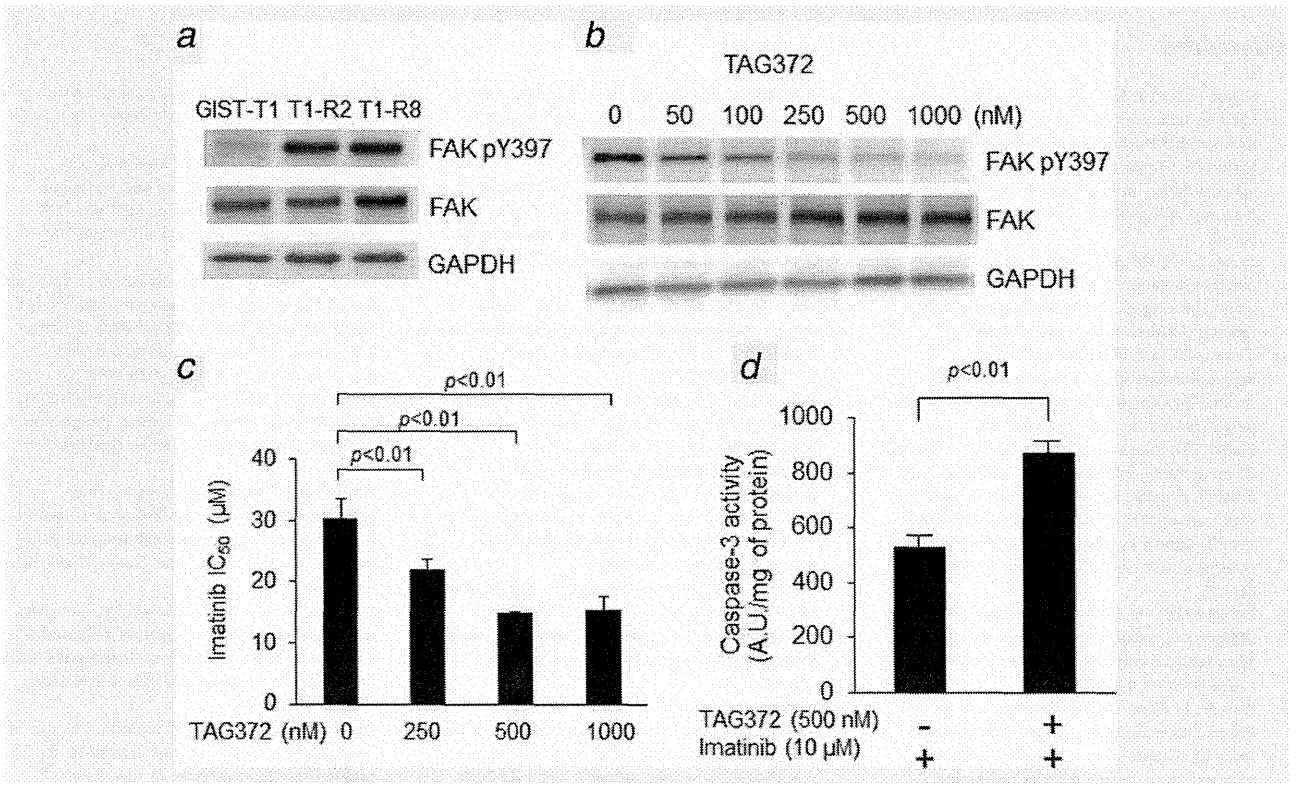

Figure 2. (*a*) Constitutive phosphorylation of FAK was observed in GIST-T1-R cells (GIST-T1-R2 and GIST-T1-R8). (*b*) Constitutive phosphorylation of FAK was observed in imatinib-resistant GIST-T1 cells (GIST-T1-R2), and TAG372 dose dependently inhibited this phosphorylation. (*c*) TAG372 reduced the IC_{50} of imatinib and induced apoptosis in GIST-T1-R2 cells. (*d*) TAG372 induced apoptosis in GIST-T1-R2 cells. Data are presented as means ± SD.

shRNA silencing of FYN induced additional cell death in GIST-T1 cells during imatinib treatment, dasatinib (a SRC family kinase inhibitor) had no effect in combination with imatinib (data not shown). These results suggest the involvement of FYN in alternative survival signaling pathways.

FAK is also a nonreceptor tyrosine kinase that is activated through autophosphorylation at Tyr^{397} by integrin and growth factor receptors; this is followed by subsequent activation of other functional phosphorylation sites to transduce the signals to downstream pathways.[22,23] FAK is reportedly overexpressed in malignant GISTs and correlated with recurrence.[19] Furthermore, FAK phosphorylation is associated with imatinib-resistance of a KIT exon 17 mutation, but not exon 11 mutation.[20] This imatinib-resistance was diminished by TAE226, which inhibits FAK and insulin-like growth factor-1 receptor. Our findings showed that imatinib induced time-dependent FAK activation in GIST-T1 cells with an imatinib-sensitive mutation of KIT exon 11. Moreover, FAK inhibition using either a FAK-specific TAG372 inhibitor or siRNA decreased the viability of GIST-T1 cells under imatinib treatment. TAG372 also induced apoptosis in imatinib-resistant cell lines with FAK activation. Taken together, it appears that FAK activation may be a critical survival signal of GIST cells under imatinib treatment, and targeting FAK with imatinib may be a promising therapeutic approach.

When imatinib was removed, KIT was quickly rephosphorylated, and FYN and FAK were simultaneously dephosphorylated (data not shown), suggesting that alternative pathway activation is functional during imatinib treatment, and may not be accompanied with qualitative changes, such as new mutations. FYN inhibition was accompanied with a subsequent lack of FAK activation, while FAK inhibition resulted in increased FYN phosphorylation, thus indicating that FYN acted upstream of FAK. However, the critical changes that induce FYN activation and subsequent FAK phosphorylation remain unknown. Additional studies are required to elucidate the FYN activation mechanisms and the alternative pathways induced by imatinib, as well as their association with acquired drug resistance.

In summary, here we found that imatinib induced increased tyrosine phosphorylation of FYN and FAK in GIST-T1 cells. Blockade of these tyrosine kinases might be a potential target to overcome imatinib resistance. Additionally, iTRAQ-based quantitative phosphotyrosine-focused proteomic analysis appears to be a useful approach to screening for phosphoproteins associated with drug resistance.

Acknowledgments

This study was partly supported by grants from Novartis Pharmaceuticals.
Conflict of interest: N.T. has honoraria to disclose from the Novatis, Pfizer and Bayer within past 2 years.

References

1. Hirota S, Isozaki K, Moriyama Y, et al. Gain-of-function mutations of c-kit in human gastrointestinal stromal tumors. *Science* 1998;279:577–80.
2. Nishida T, Hirota S, Taniguchi M, et al. Familial gastrointestinal stromal tumours with germline mutation of the kit gene. *Nat Genet* 1998;19:323–4.
3. Hirota S, Ohashi A, Nishida T, et al. Gain-of-function mutation of platelet-derived growth factor receptor αgene in gastrtointestinal stromal tumors. *Gastroenterology* 2003;125:660–7.
4. Verweij J, Casali PG, Zalcberg J, et al. Progression-free survival in gastrointestinal stromal tumours with high-dose imatinib: randomised trial. *Lancet* 2004;364:1127–34.
5. Blanke CD, Rankin C, Demetri GD, et al. Phase III randomized, intergroup trial assessing imatinib mesylate at two dose levels in patients with unresectable or metastatic gastrointestinal stromal tumors expressing the kit receptor tyrosine kinase: S0033. *J Clin Oncol* 2008;26:626–32.
6. Demetri GD, von Mehren M, Blanke CD, et al. Efficacy and safety of imatinib mesylate in advanced gastrointestinal stromal tumors. *N Engl J Med* 2002;347:472–80.
7. Blay JY, Le Cesne A, Ray-Coquard I, et al. Prospective multicentric randomized phase III study of imatinib in patients with advanced gastrointestinal stromal tumors comparing interruption versus continuation of treatment beyond 1 year: the French Sarcoma Group. *J Clin Oncol* 2007;25:1107–13.
8. Le Cesne A, Ray-Coquard I, Bui BN, et al. Discontinuation of imatinib in patients with advanced gastrointestinal stromal tumours after 3 years of treatment: an open-label multicentre randomised phase 3 trial. *Lancet Oncol* 2010;11:942–9.
9. Nishida T, Shirao K, Sawaki A, et al. Efficacy and safety profile of imatinib mesylate (ST1571) in Japanese patients with advanced gastrointestinal stromal tumors: a phase II study (STI571B1202). *Int J Clin Oncol* 2008;13:244–51.
10. Mann M, Ong SE, Grønborg M, et al. Analysis of protein phosphorylation using mass spectrometry: deciphering the phosphoproteome. *Trends Biotechnol* 2002;20:261–8.
11. Rush J, Moritz A, Lee KA, et al. Immunoaffinity profiling of tyrosine phosphorylation in cancer cells. *Nat Biotechnol* 2005;23:94–101.
12. Taguchi T, Sonobe H, Toyonaga S, et al. Conventional and molecular cytogenetic characterization of a new human cell line, GIST-T1, established from gastrointestinal stromal tumor. *Lab Invest* 2002;82:663–5.
13. Yokoyama T, Enomoto T, Serada S, et al. Plasma membrane proteomics identifies bone marrow stromal antigen 2 as a potential therapeutic target in endometrial cancer. *Int J Cancer* 2013;132:472–84.
14. Nishida T, Kanda T, Nishitani A, et al. Secondary mutations in the kinase domain of the KIT gene are predominant in imatinib-resistant gastrointestinal stromal tumor. *Cancer Sci* 2008;99:799–804.
15. Antonescu CR, Besmer P, Guo T, et al. Acquired resistance to imatinib in gastrointestinal stromal tumor occurs through secondary gene mutation. *Clin Cancer Res* 2005;11:4182–90.
16. Michor F, Hughes TP, Iwasa Y, et al. Dynamics of chronic myeloid leukaemia. *Nature* 2005;435:1267–70.
17. Timokhina I, Kissel H, Stella G, et al. Kit signaling through PI 3-kinase and Src kinase pathways: an essential role for Rac1 and JNK activation in mast cell proliferation. *EMBO J* 1998;17:6250–62.
18. Rossi F, Yozgat Y, de Stanchina E, et al. Imatinib upregulates compensatory integrin signaling in a mouse model of gastrointestinal stromal tumor and is more effective when combined with dasatinib. *Mol Cancer Res* 2010;8:1271–83.
19. Koon N, Schneider-Stock R, Sarlomo-Rikala M, et al. Molecular targets for tumour progression in gastrointestinal stromal tumours. *Gut* 2004;53:235–40.
20. Sakurama K, Noma K, Takaoka M, et al. Inhibition of focal adhesion kinase as a potential therapeutic strategy for imatinib-resistant gastrointestinal stromal tumor. *Mol Cancer Ther* 2009;8:127–34.
21. Linnekin D, DeBerry CS, Mou S. Lyn associates with the juxtamembrane region of c-Kit and is activated by stem cell factor in hematopoietic cell lines and normal progenitor cells. *J Biol Chem* 1997;272:2745–55.
22. Serrels A, McLeod K, Canel M, et al. The role of focal adhesion kinase catalytic activity on the proliferation and migration of squamous cell carcinoma cells. *Int J Cancer* 2012;131:287–97.
23. Cox BD, Natarajan M, Stettner MR, et al. New concepts regarding focal adhesion kinase promotion of cell migration and proliferation. *J Cell Biochem* 2006;99:35–52.

CD134 is a cellular receptor specific for human herpesvirus-6B entry

Huamin Tang[a,b], Satoshi Serada[c], Akiko Kawabata[a,b], Megumi Ota[a,b], Emi Hayashi[b], Tetsuji Naka[c], Koichi Yamanishi[d], and Yasuko Mori[a,b,1]

[a]Division of Clinical Virology, Center for Infectious Diseases, Kobe University Graduate School of Medicine, Kobe 650-0017, Japan; and Laboratories of [b]Virology and Vaccinology and [c]Immune Signal, Division of Biomedical Research, [d]National Institute of Biomedical Innovation, Osaka 567-0085, Japan

Edited* by Bernard Roizman, University of Chicago, Chicago, IL, and approved April 24, 2013 (received for review March 20, 2013)

Human herpesvirus-6B (HHV-6B) is a T lymphotropic β-herpesvirus that is clearly distinct from human herpesvirus-6A (HHV-6A) according to molecular biological features. The International Committee on Taxonomy of Viruses recently classified HHV-6B as a separate species. The primary HHV-6B infection causes exanthem subitum and is sometimes associated with severe encephalopathy. More than 90% of the general population is infected with HHV-6B during childhood, and the virus remains throughout life as a latent infection. HHV-6B reactivation causes encephalitis in immunosuppressed patients. The cellular receptor for HHV-6A entry was identified as human CD46, but the receptor for HHV-6B has not been clear. Here we found that CD134, a member of the TNF receptor superfamily, functions as a specific entry receptor for HHV-6B. A T-cell line that is normally nonpermissive for HHV-6B infection became highly susceptible to infection when CD134 was overexpressed. CD134 was down-regulated in HHV-6B–infected T cells. Soluble CD134 interacted with the HHV-6B glycoprotein complex that serves as a viral ligand for cellular receptor, which inhibited HHV-6B but not HHV-6A infection in target cells. The identification of CD134 as an HHV-6B specific entry receptor provides important insight into understanding HHV-6B entry and its pathogenesis.

viral entry | gQ1 | gQ2

Human herpesvirus-6B (HHV-6B) is a T lymphotropic β-herpesvirus (1) and is clearly distinct from human herpesvirus-6A (HHV-6A) according to their genetic and antigenic differences and their cell tropism (2–5). Recently the International Committee on Taxonomy of Viruses classified HHV-6B as a separate species.

The primary HHV-6B infection causes exanthem subitum (6) and is sometimes associated with severe encephalopathy, whereas the diseases caused by HHV-6A are still unknown. More than 90% of the general population is infected with HHV-6B during childhood, and the virus remains throughout life as a latent infection (7). HHV-6B reactivation causes encephalitis in immunosuppressed patients. HHV-6B reactivation is also associated with drug-induced hypersensitivity syndrome, and recent studies have suggested that it could be related to the severity of this disease (8, 9).

HHV-6A can infect a broader variety of human cells than HHV-6B (10), although the homology between HHV-6A and -6B is almost 90% over their entire genome (11–13). Human CD46 has been shown to be a cellular receptor of HHV-6 (14), and its viral ligand is a glycoprotein (g) complex made up of viral glycoprotein H (gH)/glycoprotein L (gL)/glycoprotein Q1 (gQ1)/glycoprotein Q2 (gQ2) (15). However, the HHV-6A gH/gL/gQ1/gQ2 complex binds to its human cellular receptor, CD46, whereas the corresponding complex of HHV-6B does not bind to it (10, 15). Moreover, anti-CD46 antibody does not block HHV-6B infection into the cells, whereas it does HHV-6A infection, indicating that the cellular receptor exists specific for HHV-6B infection. Because HHV-6B remains as a lifelong latent infection in more than 90% of the population and causes severe disease, it is important to identify its specific cellular receptor.

Here we show that CD134, a member of the TNF receptor superfamily, functions as a specific entry receptor for HHV-6B. A T-cell line that is normally nonpermissive for HHV-6B infection became highly susceptible to infection when CD134 was overexpressed. CD134 was down-regulated in HHV-6B–infected T cells. Soluble CD134 interacted with the HHV-6B glycoprotein complex that serves as a viral ligand, which inhibited HHV-6B but not HHV-6A infection in target cells. The identification of CD134 as an HHV-6B entry receptor provides important insight into understanding HHV-6B entry and its pathogenesis and for finding new targets for antiviral drug development.

Results

Construction of Soluble Glycoprotein Complex That Is a Viral Ligand for the Cellular Receptor. To search for candidate molecules for the HHV-6B receptor, we first prepared a soluble form of the HHV-6A or -6B gH/gL/gQ1/gQ2 complex, which is expressed on the viral envelope and acts as a viral ligand for the cellular receptor (15). One component of the complex, gH, is a type I membrane protein that retains the other molecules, gQ1, gQ2, and gL, on the membrane through its interaction with them. Therefore, to prepare the soluble gH/gL/gQ1/gQ2 complex, the transmembrane domain and cytoplasmic tail of gH were removed, and the ectodomain of gH was fused in-frame with Fc (the fragment crystallizable region of the human IgG1 antibody) and a His tag. The production of the soluble complex was confirmed by immunoblot analysis using antibodies for each component of the complex (Fig. S1*A*). Notably, the soluble HHV-6B gH/gL/gQ1/gQ2 complex efficiently bound to the Molt-3 cell line, which is permissive for HHV-6B infection (Fig. S1*B*), whereas it bound poorly to the SupT1 cell line, which is nonpermissive (Fig. S1*B*). In contrast, the soluble HHV-6A gH/gL/gQ1/gQ2 complex bound to both the Molt-3 and SupT1 cell lines (Fig. S1*B*), which both express CD46 on their cell surface.

Identification of Cellular Receptor Specific for HHV-6B. Next, to identify the cellular receptor for HHV-6B, we performed pull-down assays using the soluble HHV-6A or -6B gH/gL/gQ1/gQ2 complex and lysates of surface-biotinylated Molt-3 cells. As expected, the molecular masses of the streptavidin-labeled bands differed between HHV-6A and -6B (Fig. 1*A*). The band detected in the HHV-6A sample seemed to correspond to CD46, but the band in the HHV-6B sample did not (Fig. 1*A*). The corresponding band detected by silver staining was excised from the gel and subjected to LC-MS/MS analysis. The results identified CD134 as a candidate receptor molecule for HHV-6B.

Author contributions: H.T. and Y.M. designed research; H.T., S.S., A.K., M.O., E.H., T.N., and Y.M. performed research; H.T., K.Y., and Y.M. analyzed data; and H.T. and Y.M. wrote the paper.

The authors declare no conflict of interest.

*This Direct Submission article had a prearranged editor.

[1]To whom correspondence should be addressed. E-mail: ymori@med.kobe-u.ac.jp.

This article contains supporting information online at www.pnas.org/lookup/suppl/doi:10.1073/pnas.1305187110/-/DCSupplemental.